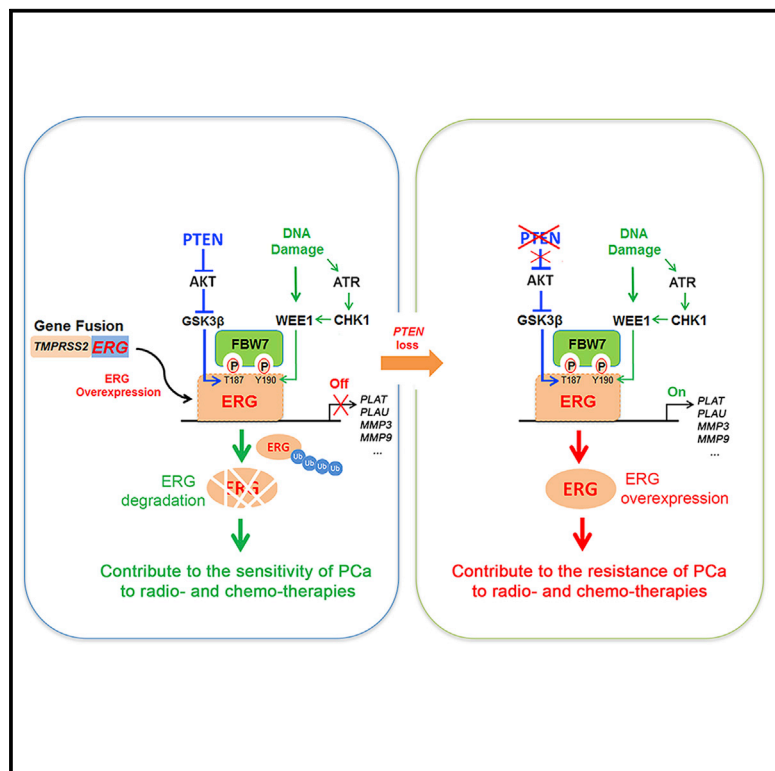


# DNA Damage Promotes TMPRSS2-ERG Oncoprotein Destruction and Prostate Cancer Suppression via Signaling Converged by GSK3 $\beta$ and WEE1

## Graphical Abstract



## Authors

Zhe Hong, Wei Zhang, Donglin Ding, ..., Qiang Wu, Denglong Wu, Haojie Huang

## Correspondence

wuqiang@tongji.edu.cn (Q.W.),  
wudenglong2009@tongji.edu.cn (D.W.),  
huang.haojie@mayo.edu (H.H.)

## In Brief

TMPRSS2-ERG oncoprotein plays a pivotal role in prostate oncogenesis and progression and is a potential therapeutic target of prostate cancer. Hong et al. reveal a previously unrecognized TMPRSS2-ERG protein destruction mechanism, and intact PTEN and GSK3 $\beta$  signaling are essential for effective targeting of TMPRSS2-ERG by genotoxic therapeutics in prostate cancer.

## Highlights

- DNA damage induces proteasomal degradation of TMPRSS2-ERG oncoprotein
- GSK3 $\beta$  and WEE1 mediates ERG T187 and Y190 phosphorylation and degradation
- FBW7 recognizes and promotes degradation of dual phosphorylated ERG
- PTEN loss confers ERG degradation and tumor growth resistance to genotoxic therapy



## Article

# DNA Damage Promotes TMPRSS2-ERG Oncoprotein Destruction and Prostate Cancer Suppression via Signaling Converged by GSK3 $\beta$ and WEE1

Zhe Hong,<sup>1,2</sup> Wei Zhang,<sup>2,3</sup> Donglin Ding,<sup>2</sup> Zhenlin Huang,<sup>2</sup> Yuqian Yan,<sup>2</sup> William Cao,<sup>2</sup> Yunqian Pan,<sup>2</sup> Xiaonan Hou,<sup>4</sup> Saravut J. Weroha,<sup>4</sup> R. Jeffrey Karnes,<sup>5,6</sup> Dejie Wang,<sup>2</sup> Qiang Wu,<sup>1,2,\*</sup> Denglong Wu,<sup>1,\*</sup> and Haojie Huang<sup>2,5,6,7,\*</sup>

<sup>1</sup>Department of Urology, Tongji Hospital, Tongji University School of Medicine, Shanghai 200065, China

<sup>2</sup>Department of Biochemistry and Molecular Biology, Mayo Clinic College of Medicine and Science, Rochester, MN 55905, USA

<sup>3</sup>Basic Medical College, Jilin Medical University, Jilin, Jilin 132013, China

<sup>4</sup>Department of Oncology, Mayo Clinic College of Medicine, Rochester, MN 55905, USA

<sup>5</sup>Department of Urology, Mayo Clinic College of Medicine and Science, Rochester, MN 55905, USA

<sup>6</sup>Mayo Clinic Cancer Center, Mayo Clinic College of Medicine and Science, Rochester, MN 55905, USA

<sup>7</sup>Lead Contact

\*Correspondence: [wuqiang@tongji.edu.cn](mailto:wuqiang@tongji.edu.cn) (Q.W.), [wudenglong2009@tongji.edu.cn](mailto:wudenglong2009@tongji.edu.cn) (D.W.), [huang.haojie@mayo.edu](mailto:huang.haojie@mayo.edu) (H.H.)  
<https://doi.org/10.1016/j.molcel.2020.07.028>

## SUMMARY

*TMPRSS2-ERG* gene fusion occurs in approximately 50% of cases of prostate cancer (PCa), and the fusion product is a key driver of prostate oncogenesis. However, how to leverage cellular signaling to ablate *TMPRSS2-ERG* oncoprotein for PCa treatment remains elusive. Here, we demonstrate that DNA damage induces proteasomal degradation of wild-type ERG and *TMPRSS2-ERG* oncoprotein through ERG threonine-187 and tyrosine-190 phosphorylation mediated by GSK3 $\beta$  and WEE1, respectively. The dual phosphorylation triggers ERG recognition and degradation by the E3 ubiquitin ligase FBW7 in a manner independent of a canonical degron. DNA damage-induced *TMPRSS2-ERG* degradation was abolished by cancer-associated PTEN deletion or GSK3 $\beta$  inactivation. Blockade of DNA damage-induced *TMPRSS2-ERG* oncoprotein degradation causes chemotherapy-resistant growth of fusion-positive PCa cells in culture and in mice. Our findings uncover a previously unrecognized *TMPRSS2-ERG* protein destruction mechanism and demonstrate that intact PTEN and GSK3 $\beta$  signaling are essential for effective targeting of ERG protein by genotoxic therapeutics in fusion-positive PCa.

## INTRODUCTION

Prostate cancer (PCa) is the most commonly diagnosed cancer among men and is the second leading cause of cancer-related death among men in Western countries (Siegel et al., 2016). There are a few options for treatment of localized PCa, such as surgery and radiation therapy. Androgen deprivation therapy (ADT) is the mainstay of treatment for advanced PCa. However, disease in the majority of patients relapses into castration-resistant PCa (CRPC) 18–24 months after initial ADT treatment (Attard et al., 2009). Currently, there is no effective treatment available for PCa patients when the next-generation androgen signaling inhibitors such as enzalutamide (Enza) and abiraterone are unsuccessful.

Although significant progress has been made, knowledge regarding the etiology and molecular signaling driving PCa progression and therapy resistance remains very limited, imposing a tremendous challenge on curing this malignancy in the clinical setting. It has been well documented that approximately 50% of patients with PCa harbor recurrent *TMPRSS2-ERG* gene rear-

rangements, in which the 5' untranslated region (5' UTR) of the androgen receptor (AR)-regulated *TMPRSS2* gene is fused to the coding region of the ETS-related gene (*ERG*) (Kumar-Sinha et al., 2008; Cancer Genome Atlas Research Network, 2015; Tomlins et al., 2005). Fusion of the *TMPRSS2* gene to other members of the ETS family, such as *ETV1*, *ETV4*, and *ETV5*, has also been detected in PCa (Clark et al., 2007). However, *ERG* fusion is far more common than other ETS gene arrangements, accounting for up to 80% of the *TMPRSS2-ETS* gene fusions in PCa (Clark et al., 2007).

Among *TMPRSS2-ERG* rearrangements, *TMPRSS2* exon 1 fused to *ERG* exon 4 (termed T1-E4 or E4) and to *ERG* exon 5 (termed T1-E5 or E5) are the two most commonly occurring gene fusions. Although both fusion genes give rise to truncated forms of ERG protein, they keep the same key functional domains as the wild-type (WT) counterpart, including the ETS DNA binding domain and the transactivation domain (TAD) (An et al., 2015). Increasing evidence suggests that *TMPRSS2-ERG* truncated protein (e.g., ERG-E4) plays a significant role in promoting prostate oncogenesis and progression (Brandi



et al., 2018; Cai et al., 2009; Dellioux et al., 2018; Tomlins et al., 2008). Knockdown (KD) of endogenously expressed TMPRSS2-ERG inhibits the growth of prostate tumors *in vitro* and *in vivo* (Tomlins et al., 2008; Wang et al., 2008). Although transgenic expression of ERG-E4 alone induces only precursor-like lesions, its overexpression is able to drive tumorigenesis in the mouse prostate harboring other genetic lesions, such as *Pten* or *Foxo1* gene deletion (Carver et al., 2009; King et al., 2009; Klezovitch et al., 2008; Yang et al., 2017). These findings indicate that TMPRSS2-ERG not only is a key driver of prostate oncogenesis but also is a viable therapeutic target in PCa.

The F box and WD40 repeat domain-containing 7 (FBW7; also termed CDC4) protein is a tumor suppressor that inhibits cell division and proliferation (Akhoondi et al., 2007). FBW7 is inactivated by gene mutation or loss of expression in numerous human malignancies, such as breast cancer (Akhoondi et al., 2007; Ye et al., 2004). FBW7 is the substrate-binding subunit of the SKP1-CULLIN1-F box (SCF<sup>FBW7</sup>) E3 ubiquitin ligase complex. It promotes polyubiquitination and proteasomal degradation of a large spectrum of oncogenic proteins, including CYCLIN E (Ye et al., 2004), c-MYC (Welcker et al., 2005; Yada et al., 2004), NOTCH (Gupta-Rossi et al., 2001), and c-JUN (Nateri et al., 2004). Most important, the substrates of FBW7 often contain a consensus FBW7-binding degron (also termed CDC4 phospho-degron [CPD]) I/P/L-T-P-X-X-S/E (where X denotes any amino acid), in which T residue is phosphorylated simultaneously with either a phosphorylated S or E, a phosphomimicking amino acid (Aifantis et al., 2008; Welcker and Clurman, 2008).

In the present study, we demonstrate that genotoxic agents such as ionizing radiation (IR) and camptothecin (CPT) induce proteasomal degradation of TMPRSS2-ERG gene fusion product, but this effect is abrogated by loss of PTEN or inactivation of GSK3 $\beta$ . We also show that both GSK3 $\beta$  and WEE1 kinases are required for DNA damage-induced TMPRSS2-ERG protein destruction. We identify a CPD (T-P-X-X-S/E)-like motif T-P-X-Y (<sup>187</sup>TPSY<sup>190</sup>) in ERG and demonstrate that mutation of threonine-187 (T187) and tyrosine-190 (Y190) to alanine abolishes DNA damage-induced degradation of TMPRSS2-ERG. Finally, we show that expression of degradation-resistant TMPRSS2-ERG promotes genotoxic therapy-resistant growth of PCa cells in culture and in mice.

## RESULTS

### Genotoxic Therapeutic Agents Induce Proteasomal Degradation of TMPRSS2-ERG Protein

Given the critical role of TMPRSS2-ERG truncated protein in prostate tumorigenesis and progression, we sought to determine how to ablate TMPRSS2-ERG protein in ERG gene fusion-positive PCa. To this end, we used the VCaP cell line as a working model because it expresses both endogenous WT full-length ERG (ERG-FL) and truncated TMPRSS2-ERG protein (ERG-E4) (An et al., 2015). We first performed short-term treatment (8 h) of VCaP cells with therapeutic agents that are in clinical use, including Enza, docetaxel (DTX), CPT, and IR. We demonstrated that although Enza and DTX failed to affect ERG-FL protein expression, both CPT and IR treatment drasti-

cally decreased ERG-FL expression in VCaP cells (Figure 1A). Most important, whereas Enza and DTX treatment had little or no effect on ERG-E4 expression at protein and mRNA levels, both CPT and IR treatment markedly decreased its expression at protein level, but not the mRNA level (Figures 1A and 1B), suggesting that DNA damaging agents regulate ERG truncated protein expression at the posttranscriptional level. Expression of TMPRSS2-ERG fusion gene mRNA is known to be regulated by the AR. We found that at 8 h post-treatment, neither IR nor CPT treatment altered expression of AR protein and its target gene *KLK3* mRNA expression (Figures 1A and 1B), arguing that the effect of IR and CPT on ERG-E4 expression is independent of AR expression and its transcriptional activity in VCaP cells. Similar results were obtained in VCaP cells at a longer time point (24 h) after IR and CPT treatment in VCaP cells (Figures S1A and S1B). As expected, the longer time treatment of the AR inhibitor Enza not only decreased *KLK3* mRNA expression but also down-regulated ERG-E4 expression at both mRNA and protein levels (Figures S1A and S1B). We further showed that both IR and CPT treatment decreased ERG-E4 protein expression in a dose-dependent manner (Figures 1C and 1D). These data suggest that DNA damaging agents decrease ERG expression at the posttranscriptional level.

Next, we sought to determine how DNA damage regulates ERG-E4 expression at the posttranscriptional level. 22Rv1 PCa cells were transfected with hemagglutinin (HA)-tagged ERG-FL (WT), ERG-E4, or ERG-E5 and treated with CPT and/or the proteasome inhibitor MG132. The levels of different forms of ERG protein were invariably decreased upon DNA damage, but such effect was blocked by MG132 (Figures 1E and 1F). By performing *in vivo* ubiquitination assay, we showed that CPT treatment induced polyubiquitination of WT and cancer-derived ERG proteins (Figure 1G). Moreover, CPT treatment significantly shortened the half-life of both endogenous WT ERG and ERG-E4 in VCaP cells (Figures 1H–1J). These data indicate that DNA damage induces ubiquitination and proteasomal degradation of both WT and TMPRSS2-ERG truncated proteins in PCa cells. It has been reported that SPOP and TRIM25 E3 ubiquitin ligases target ERG protein for ubiquitination and proteasomal degradation in the conditions without DNA damage (An et al., 2015; Gan et al., 2015; Wang et al., 2016). As expected, KD of SPOP and TRIM25 increased the level of both endogenous WT and ERG-E4 in mock-treated VCaP cells (Figure S1C). However, SPOP and TRIM25 co-KD failed to block ERG protein degradation in CPT-treated VCaP cells (Figure S1C). These data suggest that DNA damage induces ERG degradation through a mechanism independent of SPOP and TRIM25.

### Functional GSK3 $\beta$ Is Required for DNA Damage-Induced Degradation of ERG

To define the molecular mechanism underlying DNA damage-induced ERG degradation, we surveyed CPT's effect on ERG protein expression in a panel of PCa cell lines including both PTEN-positive (22Rv1 and DU145) and PTEN-negative cell lines (LNCaP, C4-2, and PC-3), all of which do not harbor the TMPRSS2-ERG rearrangement. We first transfected HA-tagged FL, E4, and E5 ERG into these cell lines and then treated them with CPT. Similar to the finding in VCaP cells, we found that CPT treatment

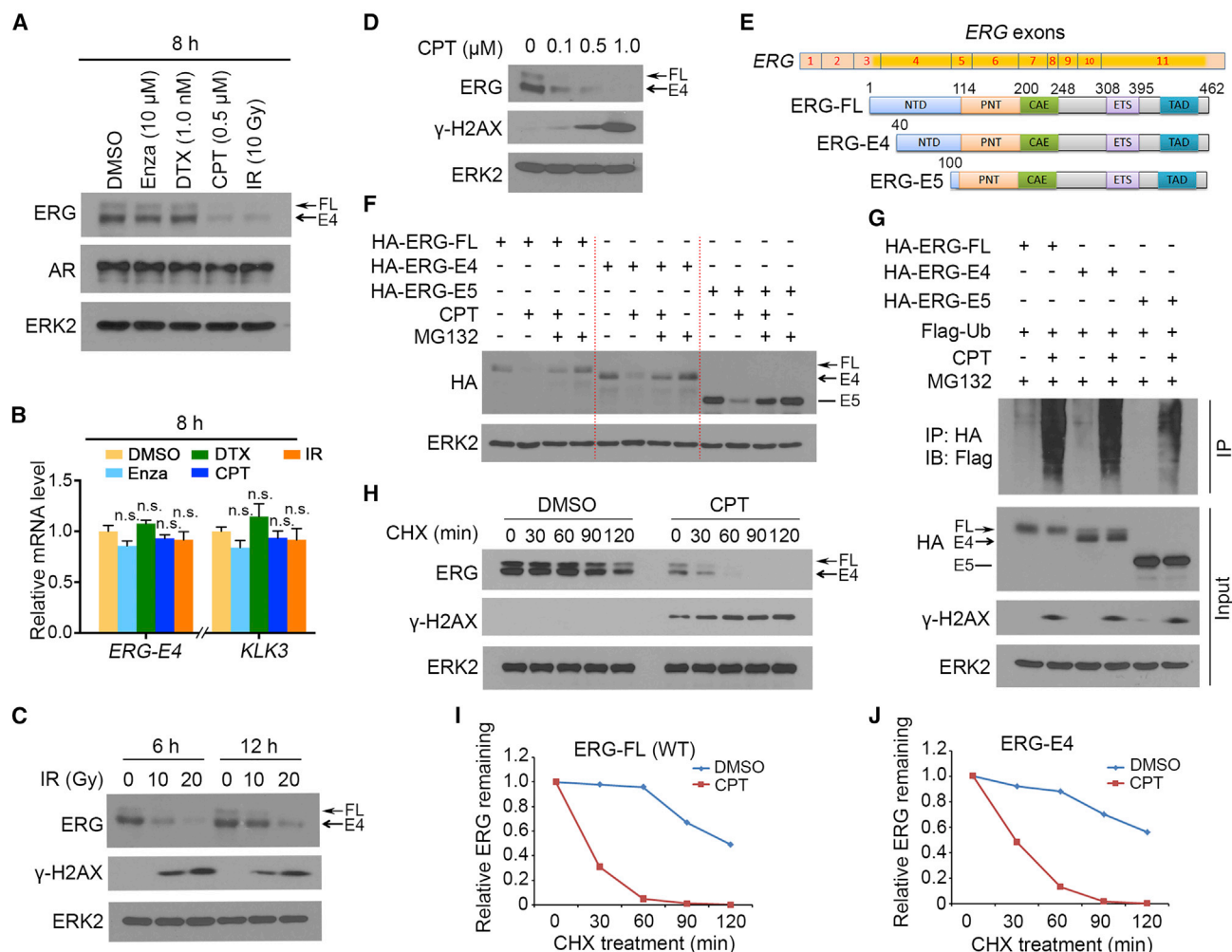


**Figure 1. Genotoxic Therapeutic Agents Induce Proteasomal Degradation of TMPRSS2-ERG Proteins**

(A and B) VCaP cells were treated as indicated for 8 h, and cells were harvested for western blot (WB) (A) and qRT-PCR (B). ERK2 serves as a loading control. FL, full-length ERG; E4, ERG-E4 protein. Data are shown as mean value  $\pm$  SD. n.s., not significant compared with mock (DMSO) treatment (unpaired two-tailed Student's *t* test).

(C) VCaP cells were irradiated with indicated dosages and cultured for indicated time periods. Cells were harvested for WB.  $\gamma$ -H2AX was included as an indicator of DNA damage.

(D) VCaP cells were treated with CPT at indicated concentrations for 8 h and harvested for WB.

(E) Schematic diagram of FL ERG and TMPRSS2-ERG fusion products E4 and E5. Different exons and the coding region (yellow) of the *ERG* gene are also indicated. The regions in blue, orange, green, purple, and dark blue colors represent NTD, PNT, CAR, ETS (DNA binding), and TAD (transactivation) domains of ERG protein, respectively.

(F and G) Plasmids for HA-tagged FL, E4, and E5 were transfected into 22Rv1 cells and treated with or without CPT (0.5  $\mu$ M) and MG132 (20  $\mu$ M) for 8 h, followed by WB (F) or IP with anti-HA antibody and WB with indicated antibodies (G).

(H) VCaP cells were treated with or without CPT (0.5  $\mu$ M) for 6 h and then treated in combination with cycloheximide (CHX) (50  $\mu$ g/mL). Cells were harvested at the indicated time points for WB.

(I and J) Western blots in (H) were quantified and normalized with the value of the 0 min time point and are shown as line graphs for ERG-FL (I) and ERG-E4 (J).

decreased expression of both FL and truncated ERG proteins in 22Rv1 cell line, but not in the other four cell lines (Figure 2A). As expected, AKT was readily phosphorylated (e.g., at serine-473 [S473]) in PC-3, LNCaP, and C4-2 PTEN-negative cell lines, but not in 22Rv1, DU145, and VCaP PTEN-positive cell lines (Figure 2B). GSK3 $\beta$  is a downstream kinase of AKT, and GSK3 $\beta$  phosphorylation at serine-9 (S9) by AKT and other members of the AGC kinase family results in the loss of function of GSK3 $\beta$  (van Weeren

et al., 1998). We found that GSK3 $\beta$  S9 phosphorylation was correlated with AKT phosphorylation among these cell lines except the PTEN-positive cell line DU145, where GSK3 $\beta$  S9 phosphorylation level was comparable with that in three PTEN-negative cell lines (Figure 2B). Because DNA damage decreases ERG protein expression only in GSK3 $\beta$ -unphosphorylated PCa cell lines (Figures 1, 2A, and 2B), our data suggest that active GSK3 $\beta$  is critical for ERG protein destruction induced by DNA damage.

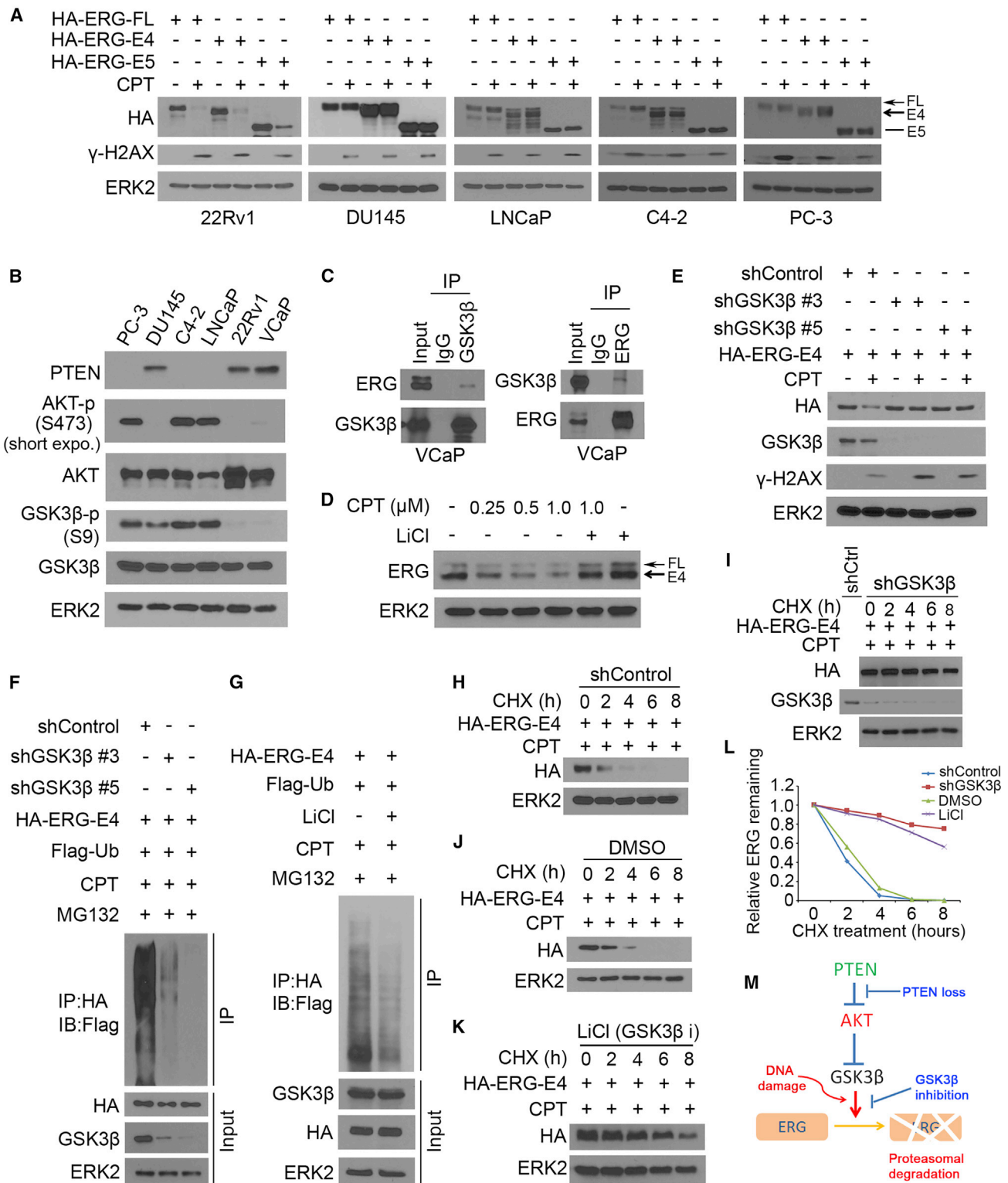


**Figure 2. Functional GSK3β Is Required for DNA Damage-Induced Degradation of ERG**

(A) Plasmids for HA-tagged FL, E4, and E5 ERG were transfected into 22Rv1, DU145, LNCaP, C4-2, and PC-3 cell lines and treated with or without CPT (0.5 μM) for 8 h. Cells were harvested for western blot (WB). ERK2 serves as a loading control.

(B) Indicated PCa cell lines were cultured and harvested for WB with indicated antibodies.

(legend continued on next page)

To determine the precise role of GSK3 $\beta$  in ERG protein degradation, we performed coIP assay to explore whether GSK3 $\beta$  interacts with ERG in degradation-responsive VCaP cells. Reciprocal coIP assays showed that GSK3 $\beta$  interacts with ERG at the endogenous level (Figure 2C). The importance of GSK3 $\beta$  in ERG degradation is further manifested by our observation that the treatment of the GSK3 $\beta$  inhibitor lithium chloride (LiCl) blocked CPT-induced ERG protein destruction in VCaP cells (Figure 2D). KD of endogenous GSK3 $\beta$  by two independent small hairpin RNAs (shRNAs) also abrogated CPT-induced ERG degradation (Figure 2E). Moreover, both GSK3 $\beta$  KD and LiCl treatment invariably inhibited CPT-induced polyubiquitination of ERG-E4 (Figures 2F and 2G) and prolonged the half-life of this protein (Figures 2H–2L). These data indicate that active GSK3 $\beta$  is essential for DNA damage-induced proteasomal degradation of ERG in PCa cells, but this role of GSK3 $\beta$  is surrendered because of genetic alterations (e.g., S9 phosphorylation-mediated inactivation of GSK3 $\beta$  due to PTEN loss (AKT activation) or pharmacological inhibition (Figure 2M).

#### AKT Inhibition Restores DNA Damage-Induced ERG Degradation in PTEN-Null Cells *In Vitro* and *In Vivo*

To further investigate the importance of an active GSK3 $\beta$  in DNA damage-induced ERG degradation, we first assessed whether endogenous ERG is a phosphorylation target of GSK3 $\beta$  in PCa cells. To this end, we transfected WT and the constitutively active (AKT/AGC kinase phosphorylation-resistant) GSK3 $\beta$  mutant S9A (GSK3 $\beta$ -S9A) into VCaP cells. We demonstrated that GSK3 $\beta$ -S9A expression increased endogenous ERG phosphorylation in VCaP cells, and ERG phosphorylation inversely correlated with total ERG level (Figures S1D and S1E). We further examined the effect of GSK3 $\beta$ -S9A in PTEN-negative LNCaP cells in which endogenous GSK3 $\beta$  is inactive because of S9 phosphorylation (Figure 2B). GSK3 $\beta$ -S9A expression restored DNA damage-induced polyubiquitination and degradation of the cancer-derived ERG-E4 oncoprotein in this cell line (Figures 3A and 3B). As AKT activation suppresses GSK3 $\beta$  activity (Her-mida et al., 2017), we examined the impact of AKT inhibition on DNA damage-induced ERG degradation in PTEN-negative cells. The treatment of PTEN-null C4-2 cells with the AKT inhibitor MK2206 resumed CPT-induced polyubiquitination and degradation of ERG-E4 protein (Figures 3C and 3D). Although as expected, serum starvation decreased AKT and GSK3 $\beta$  phosphor-

ylation in VCaP cells, it also enhanced ERG degradation caused by DNA damage (Figure 3E). However, these processes were completely reversed by IGF-1 treatment (Figure 3E).

Next, we examined whether inactivation of AKT enables restoration of CPT-induced ERG protein degradation and PCa growth inhibition *in vivo*. To this end, we used a novel *Pb-Cre;ERG-E4<sup>Rosa26-loxP-stop-loxP</sup>;Pten<sup>loxP/loxP</sup>;Trp53<sup>loxP/R172H</sup>* (termed Rosa-EPT) genetically engineered mouse (GEM) model generated by crossbreeding Probasin-Cre (*Pb-Cre4*) mice with conditional Rosa26 locus-specific *ERG-E4* transgenic mice, conditional *Pten<sup>loxP/loxP</sup>* mice, and *Trp53*-knockout/R172H-knockin mice. Similar to our previous findings in the Probasin-driven *ERG-E4;Pten* knockout/*Trp53*-knockout/R172H-knockin (*Pb-EPT*) model (Blee et al., 2018), Rosa-EPT mice developed AR-positive prostate adenocarcinoma at 6 months of age (Z. Huang and H. Huang, unpublished data), indicating that the Rosa-EPT model is suitable for further studies of the effect of PTEN loss on ERG degradation *in vivo*. We transplanted Rosa-EPT tumors into SCID mice and treated mice with vehicle, CPT-11 (irinotecan, a CPT derivative in clinical use), GDC0068 (an AKT inhibitor in a clinical trial; Saura et al., 2017), or both. Although treatment of tumors with either CPT-11 or GDC0068 alone had limited inhibitory effect on growth of Rosa-EPT tumors, combined treatment of CPT-11 and GDC0068 largely blocked tumor growth (Figures 3F–3H). In concordance with the findings, co-treatment of CPT-11 and GDC0068 completely abolished ERG-E4 expression in tumors, although each treatment alone failed to decrease ERG-E4 protein level (Figure 3I). The growth-inhibitory effect of the co-treatment with CPT-11 and GDC0068 was corroborated with downregulation of Ki67 and upregulation of cleaved caspase-3 (Figures 3I–3K). Together, we provide both *in vitro* and *in vivo* evidence that pharmacological inhibition of AKT can restore genotoxic agent-induced TMPRSS2-ERG oncoprotein destruction and growth inhibition of PTEN-deficient PCa (Figure 3L).

#### Activation of CHK1 and WEE1 Promotes ERG Degradation in Response to DNA Damage

Our finding that constitutively active GSK3 $\beta$ -S9A induces ERG protein degradation only under DNA damage conditions (Figure 3A) prompted us to determine which DNA damage signaling pathway protein(s) are required for ERG protein destruction. Components of DNA damage response (DDR) pathways, which

(C) VCaP cells were treated with CPT (0.5  $\mu$ M) and MG132 (20  $\mu$ M) for 8 h. Cells were harvested for reciprocal co-IP assays using GSK3 $\beta$  antibody and ERG antibody followed by WB.

(D) VCaP cells were treated with or without LiCl (2 mM) and CPT at different doses for 8 h followed by WB.

(E) Control or GSK3 $\beta$ -specific knockdown 22Rv1 cells were transfected with HA-ERG-E4 plasmid and treated with or without CPT (0.5  $\mu$ M) for 8 h. Cells were harvested for WB.

(F) Control or GSK3 $\beta$ -specific knockdown 22Rv1 cells were transfected with indicated plasmids and treated with CPT (0.5  $\mu$ M) and MG132 (20  $\mu$ M) for 8 h. Cells were harvested for IP and WB.

(G) 22Rv1 cells were transfected with the indicated plasmids and treated with CPT (0.5  $\mu$ M) and MG132 (20  $\mu$ M) in combination with or without LiCl (2 mM) for 8 h. Cells were harvested for IP and WB.

(H and I) Control (H) or GSK3 $\beta$ -specific knockdown (I) 22Rv1 cells were transfected with the indicated plasmids and treated with CPT (0.5  $\mu$ M) and cycloheximide (CHX) (50  $\mu$ g/mL). Cells were harvested at the indicated time points for WB.

(J and K) 22Rv1 cells were transfected with the indicated plasmids and treated with CPT (0.5  $\mu$ M) and CHX (50  $\mu$ g/mL) in combination with DMSO (J) or LiCl (2 mM) (K). Cells were harvested for WB at the indicated time points.

(L) Western blots in (H)–(K) were quantified and normalized with the value of the 0 h time point and are shown as a line graph.

(M) A schematic diagram shows the role of GSK3 $\beta$  in ERG protein degradation in response to DNA damage.

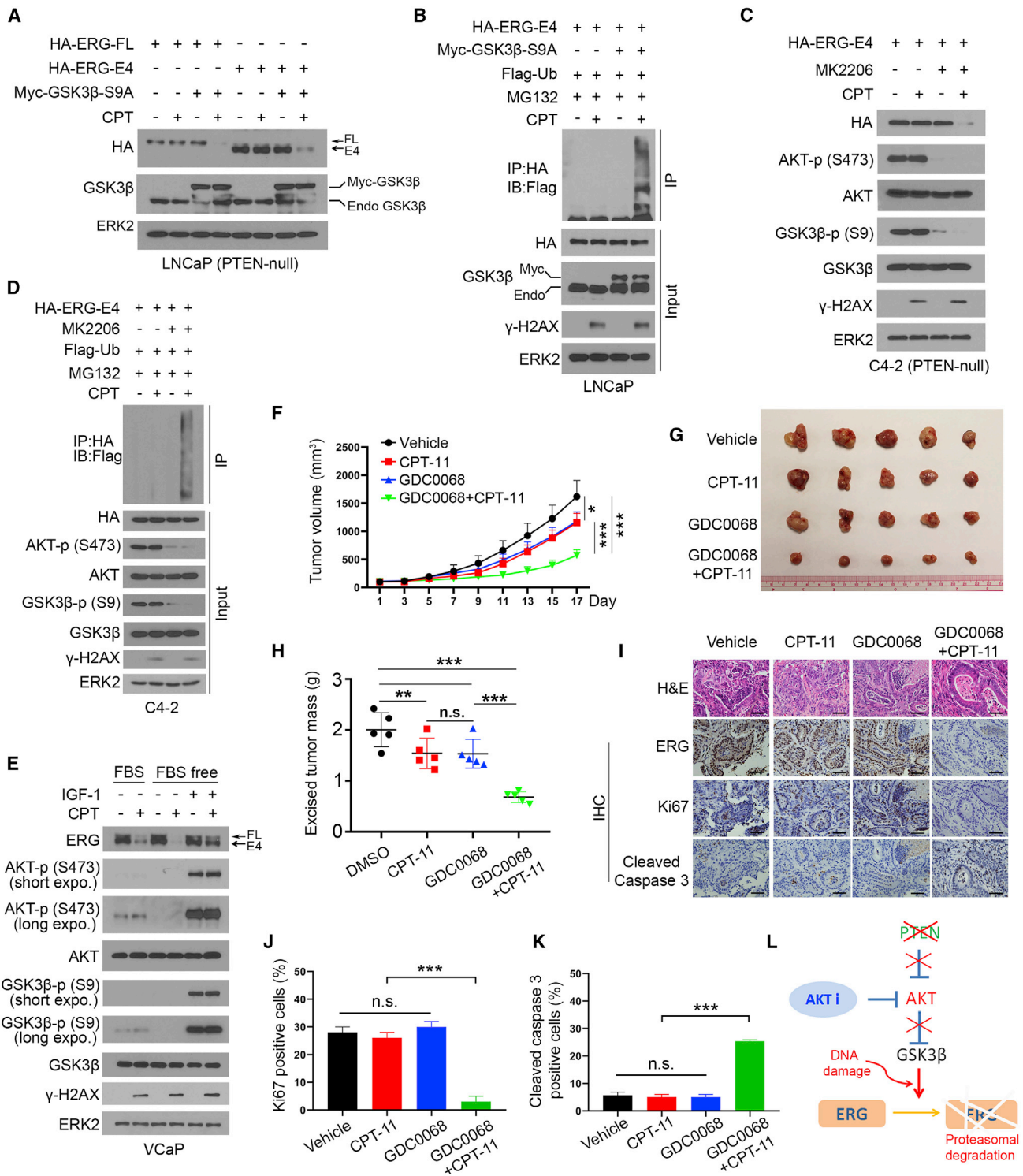


**Figure 3. AKT Inhibition Restores DNA Damage-Induced ERG Degradation in PTEN-Null Cells in Culture and in Mice**

(A) PTEN-null LNCaP cells were transfected with the indicated plasmids and treated with or without CPT (0.5  $\mu$ M) for 8 h followed by western blot (WB). ERK2 serves as a loading control.  
(B) LNCaP cells were transfected with the indicated plasmids and treated with MG132 (20  $\mu$ M) and CPT (0.5  $\mu$ M) for 8 h. Cells were harvested for immunoprecipitation (IP) and WB.  
(C) PTEN-null C4-2 cells were transfected with the indicated plasmids and treated with or without CPT (0.5  $\mu$ M) and MK2206 (0.5  $\mu$ M) for 8 h followed by WB.

(legend continued on next page)

include ATM, ATR, CHK1, CHK2, and WEE1, play important roles in initiating, transducing, and executing cellular responses to DNA damage (Carrassa and Damia, 2017; Grabocka et al., 2015; Lee et al., 2001; Lin et al., 2017; Maréchal and Zou, 2013; Smith et al., 2010). We treated 22Rv1 cells with CPT in combination with the inhibitor for ATM, ATR, CHK1/CHK2, or WEE1. We demonstrated that except the ATM inhibitor Ku-55933, the ATR inhibitor VE-822, the CHK1 and CHK2 dual inhibitor AZD7762, or the WEE1 inhibitor MK1775 abrogated CPT-induced ERG degradation (Figure 4A), suggesting that these kinases might take part in ERG degradation. In agreement with these observations, CHK1 KD by two independent shRNAs partially but ATR or WEE1 KD almost completely abolished ERG destruction under DNA damage conditions (Figures 4B–4F). Accordingly, both CPT and radiation treatment induced CHK1 phosphorylation and activation (Figures 4G and 4H). Furthermore, CHK1 or WEE1 KD diminished ERG polyubiquitination in CPT-treated 22Rv1 cells (Figures 4I and 4J). CHK1 or WEE1 KD also prolonged ERG protein half-life in 22Rv1 cells, and similar results were obtained in cells treated with the inhibitor of these proteins (Figures 4K–4R). Collectively, our data suggest that WEE1 and its upstream activator CHK1 are crucial for ERG protein degradation in response to DNA damage.

### FBW7 Mediates ERG Degradation in Response to DNA Damage

After demonstrating the role of GSK3 $\beta$  and the CHK1-WEE1 axis in DNA damage-induced destruction of ERG protein, we sought to identify the E3 ubiquitin ligase responsible for this process. Proteins phosphorylated by GSK3 $\beta$  are often the ubiquitination substrates of  $\beta$ -TrCP1 and FBW7 E3 ligases (Minella and Clurman, 2005; Robertson et al., 2018; Shimizu et al., 2018). The  $\beta$ -TrCP1 degradation substrates usually harbor a consensus phosphodegron DpSGXXpS (the lowercase p indicates phosphorylated S, and X represents any amino acid) (Fuchs et al., 2004). Protein sequence analysis revealed that ERG protein does not contain any consensus  $\beta$ -TrCP1 degron motif DSGXXS. Next, we analyzed ERG protein sequence by searching for a canonical phosphodegron (L/I/PpTPXXpS/T or L/I/PpTPXXE) of FBW7 (the lowercase p indicates phosphorylated T/S, and X represents any amino acid except K or R) (Hong et al., 2016). Although we could not find any consensus FBW7 phosphodegron motif in ERG, we did notice a variant motif, <sup>186</sup>LTPSY<sup>190</sup>, which is similar to an atypical FBW7 degron implicated in Polo-like kinase 1 (PLK1) (Giráldez et al., 2014) (Figure 5A). This motif is evolutionally conserved among different

species (Figure 5B), suggesting that it might be a functionally important motif targeted by FBW7.

To define the role of FBW7 in ERG protein degradation, we first examined whether FBW7 binds to ERG by performing reciprocal coIP assays. We found that FBW7 interacted with both WT and E4 ERG at the endogenous level in VCaP cells (Figure 5C). We also showed that FBW7 bound with ectopically expressed HA-tagged WT, E4, and E5 ERG in 22Rv1 cells (Figure S1F). Importantly, DNA damage-induced ERG protein degradation was completely abolished by FBW7 KD (Figure 5D). In contrast, FBW7 overexpression induced ERG protein degradation in a dose-dependent manner in CPT-treated 22Rv1 cells (Figure 5E). A similar dose effect of FBW7 on ERG protein destruction was observed in VCaP cells, and such effect was DNA damage dependent (Figure 5F), further underscoring the importance of DNA damage signaling in ERG degradation. *In vivo* ubiquitination assay showed that FBW7 KD by two independent shRNAs abolished ERG protein ubiquitination in both VCaP and 22Rv1 cells (Figures 5G and S1G). In contrast, FBW7 overexpression substantially increased ERG polyubiquitination (Figure 5H). Furthermore, FBW7 KD prolonged, but FBW7 overexpression shortened, ERG protein half-life (Figures 5I–5L). Taken together, these data suggest that the E3 ubiquitin ligase FBW7 plays an important role in DNA damage-induced degradation of ERG protein in PCa cells.

### T187 and Y190 Phosphorylation Is Crucial for ERG Degradation

Thus far, our data indicate that GSK3 $\beta$  and WEE1 kinases and FBW7 ligase are required for DNA damage-induced degradation of ERG protein (Figures 4 and 5). FBW7 normally binds to two phosphorylation sites within the degron motif of its substrates (Figure 5A). GSK3 $\beta$  belongs to the family of proline-directed protein kinases that phosphorylate serine or threonine residues preceding proline (S/TP) (Lu et al., 2002). Human WEE1 is a tyrosine (Y)-specific protein kinase (Parker and Pivnicka-Worms, 1992). On the basis of our data and findings in the literature, we hypothesized that T187 and Y190 in the FBW7 phosphodegron variant motif <sup>186</sup>LTPSY<sup>190</sup> are putative GSK3 $\beta$  and WEE1 phosphorylation sites, respectively (Figure 5A).

To test this hypothesis, we first examined whether DNA damage induces FBW7-ERG interaction in a phosphorylation-dependent manner. We demonstrated that FBW7 only interacted with ERG-E4 in CPT-treated 22Rv1 cells (Figure 6A), and such interaction was phosphorylation dependent, as  $\lambda$  phosphatase treatment of cell lysate completely abrogated their binding

(D) C4-2 cells were transfected with the indicated plasmids and treated with or without CPT (0.5  $\mu$ M), MK2206 (0.5  $\mu$ M), and/or MG132 (20  $\mu$ M) for 8 h. Cells were harvested for IP and WB.

(E) VCaP cells cultured in regular medium or serum-starved VCaP cells were pre-treated with or without IGF-1 (100 ng/mL), followed by treatment with or without CPT (0.5  $\mu$ M) for 8 h. Cells were harvested for WB.

(F–H) Allografts generated from Rosa-EPT mice were treated with CPT-11 (10 mg/kg, every 2 days) or GDC0068 (50 mg/kg, 5 days a week) or their combination, and tumor growth was measured (F). Tumors were harvested at day 17 and photographed (G), and tumor weight (H) was measured. Data are shown as mean value  $\pm$  SD. \* $p$  < 0.05, \*\*\* $p$  < 0.001, and n.s., not significant (unpaired two-tailed Student's  $t$  test).

(I) H&E staining and IHC staining for ERG, Ki67, and cleaved caspase-3 were performed. Representative images were taken from each group ( $n$  = 5). Scale bars are indicated in the images. Scale bar: 50  $\mu$ m.

(J and K) Ki67 (J) and cleaved caspase-3 (K) positive cells in tissues obtained from (G) were quantified. The number of positive cells from at least five fields was counted and analyzed. Data are shown as mean value  $\pm$  SD. \*\*\* $p$  < 0.001 and n.s., not significant (unpaired two-tailed Student's  $t$  test).

(L) Schematic diagram showing the effect of the AKT inhibitor (AKTi) in restoring DNA damage-induced ERG degradation in PTEN-null cells.

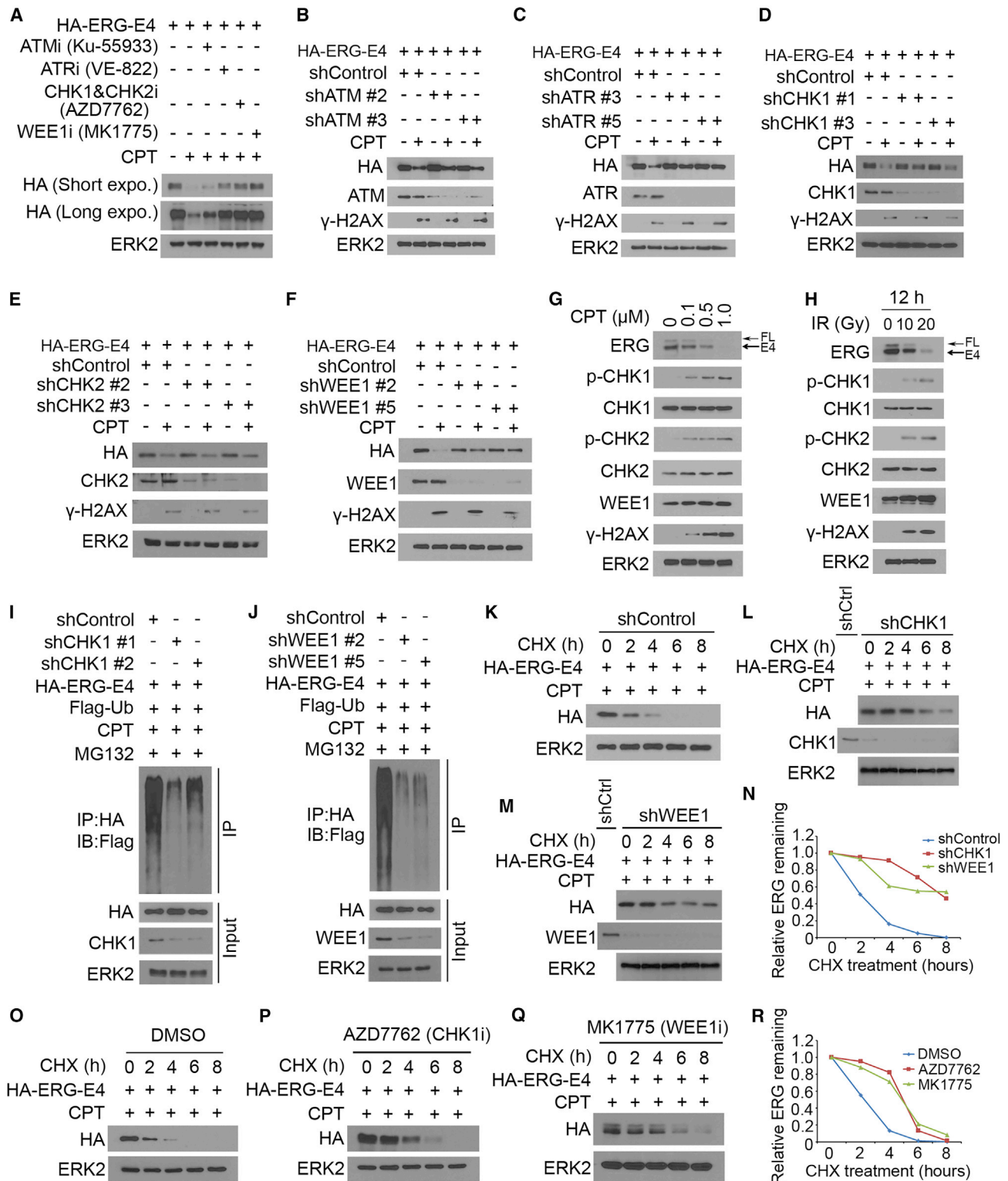


**Figure 4. Activation of CHK1 and WEE1 Promote ERG Degradation in Response to DNA Damage**

(A) 22Rv1 cells transfected with HA-ERG-E4 were pre-treated with indicated inhibitors of components of the DNA damage response pathway, including Ku-55933 (1  $\mu$ M), VE-822 (3  $\mu$ M), AZD7762 (1.5  $\mu$ M), and MK1775 (1  $\mu$ M), for 12 h followed by treatment with CPT (0.5  $\mu$ M) for 8 h. Cells were harvested for WB. ERK2 serves as a loading control.

(legend continued on next page)

(Figure 6B). These data support the notion that ERG phosphorylation is required for DNA damage-induced interaction between ERG and FBW7. Moreover, we performed an *in vitro* kinase assay using ERG-E4 glutathione-S-transferase (GST) recombinant protein as the substrate. We demonstrated that WEE1 alone was sufficient to phosphorylate ERG and the phosphorylation was abolished by Y190A mutation (Figures 6C and 6D), indicating that WEE1 phosphorylates ERG at Y190 *in vitro*. In contrast, we found that GSK3 $\beta$  alone was insufficient to phosphorylate ERG and that GSK3 $\beta$  was able to phosphorylate ERG in the presence of WEE1, but this effect was abrogated by T187A mutation (Figures 6C and 6D). These results are not only consistent with the finding that GSK3 $\beta$  can phosphorylate ERG at the endogenous level in cells (Figures S1D and S1E), but also indicate that T187 phosphorylation of ERG by GSK3 $\beta$  is primed by WEE1 phosphorylation on Y190, and this observation is consistent with findings in the literature that GSK3 $\beta$  is a kinase requiring priming phosphorylation.

To determine the role of T187 and Y190 phosphorylation in DNA damage-induced ERG protein destruction, we generated phosphorylation-resistant or phosphorylation-mimicking mutants for both T187 (T187A and T187D) and Y190 (Y190A and Y190D) (Figure 6E). We demonstrated that T187A abolished FBW7 interaction with ERG-E4 in 22Rv1 cells, while T187D enhanced FBW7-ERG interaction (Figure 6F). Similar results were observed for the Y190A and Y190D mutants (Figure 6G). In agreement with these observations, both GSK3 $\beta$  KD and WEE1 KD abolished FBW7 interaction with unmutated ERG-E4, but the interaction of FBW7 with T187D and Y190D ERG mutants was unaffected (Figures 6H and 6I). Collectively, these data indicate that phosphorylation of T187 and Y190 is a prerequisite for DNA damage-induced degradation of ERG. They also suggest that GSK3 $\beta$  and WEE1 are the two major kinases responsible for T187 and Y190 phosphorylation, respectively.

### Both DNA Damage and FBW7 Expression Can Inhibit ERG Target Gene Transcription

ERG is a transcription factor that exerts the oncogenic function primarily through transactivating the downstream target genes (Adamo and Ladomery, 2016; Brenner et al., 2011). *MMP9* is a well-studied ERG transcriptional target (Tian et al., 2014). We first performed an *MMP9* promoter-based luciferase reporter assay to determine whether DNA damage and FBW7 could influence the *MMP9* transcription. CPT treatment decreased the activity of the *MMP9* reporter gene, and the repression effect was further enhanced by ectopic expression of FBW7 (Figure S2A).

We next examined how CPT treatment and FBW7 overexpression affect expression of ERG target genes, including *PLAU*, *PLAT*, *MMP3*, and *MMP9* (Tomlins et al., 2008). CPT treatment decreased the expression of these genes at the mRNA level in 22Rv1 cells (Figures S2B–S2E). Chromatin immunoprecipitation-coupled quantitative PCR (ChIP-qPCR) assays showed that CPT treatment, in combination with or without FBW7 expression, reduced ERG binding at the promoters of *PLAU*, *PLAT*, *MMP3*, and *MMP9* genes, and these results were consistent with the level of ERG-E4 protein (Figures S2F–S2J). Thus, DNA damage and FBW7 expression act in concert to inhibit the transcriptional activity of ERG in PCa cells.

### Degradation-Resistant ERG Confers Resistance to Genotoxic Treatment of PCa Cells in Culture and in Mice

To determine how ERG degradation affects PCa cell growth in response to DNA damage, we depleted endogenous ERG in VCaP cells using ERG-specific shRNAs and restored with shRNA-resistant unmutated ERG-E4, ERG-E4-T187A, or ERG-E4-Y190A mutant (Figure 7A). The MTS assays showed that control and ERG-E4 re-expressing cells were very sensitive to CPT treatment; however, ERG-E4-T187A- and ERG-E4-Y190A-expressing cells were largely resistant (Figures 7B–7E). Similar results were obtained from colony formation assays (Figures 7A, 7F, and 7G). Importantly, depletion of endogenous ERG-E4 in VCaP cells impaired the sensitivity to CPT treatment, as demonstrated in MTS and colony formation assays (Figures 7F, 7G, and S3A), and this effect seems CPT specific, as no such effect was observed for other anti-cancer agents, such as DTX and Enza, in both VCaP and 22Rv1 cells (Figures S3A–S3F). Consistent with the results obtained from *in vitro* assays, we found that CPT-11 treatment markedly inhibited the growth ERG-E4-positive VCaP tumors in mice, but a further additive effect was observed after concomitant KD of ERG-E4 (Figures 7H–7J). However, the inhibitory effect of CPT-11 was largely abolished by restored expression of degradation-resistant ERG-E4-Y190A, but not unmutated ERG-E4 (Figures 7H–7J). These results are consistent with the expression of Ki67 and cleaved caspase-3 in the tumors of different groups (Figures 7K–7M). Furthermore, we repeated these experiments in ERG-E4-negative 22Rv1 cells by introducing unmutated ERG-E4 or degradation-resistant ERG-E4-T187A or ERG-E4-Y190A, and we obtained similar *in vitro* and *in vivo* results (Figures S4A–S4M). Together, our data indicate that blocking GSK3 $\beta$  and/or WEE1-mediated ERG protein degradation confers resistance to DNA targeted genotoxic treatment of PCa cells *in vitro* and *in vivo*.

(B–F) 22Rv1 cells stably expressing control shRNA or gene-specific shRNA for ATM (B), ATR (C), CHK1 (D), CHK2 (E), or WEE1 (F) were transfected with HA-ERG-E4. Cells were treated with or without CPT (0.5  $\mu$ M) for 8 h followed by WB.

(G and H) VCaP cells were treated with CPT for 8 h (G) or IR (H) and harvested for WB.

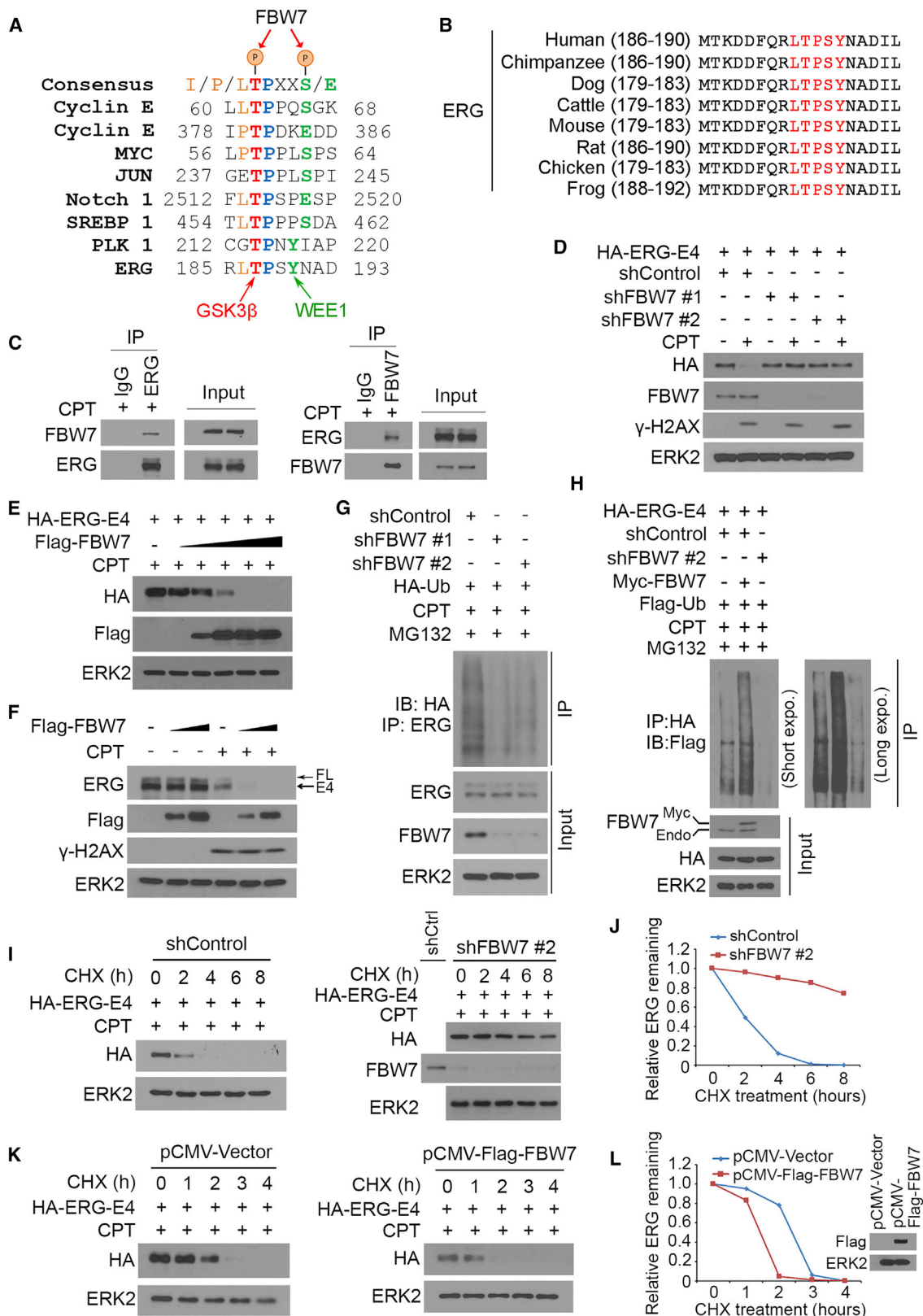
(I and J) 22Rv1 cells stably expressing control shRNA or gene-specific shRNA for CHK1 (I) and WEE1 (J) were transfected with HA-ERG-E4 and FLAG-Ub and treated with CPT (0.5  $\mu$ M) and MG132 (20  $\mu$ M) for 8 h followed by IP and WB.

(K–M) Control, CHK1, or WEE1 knockdown 22Rv1 cells were transfected with HA-ERG-E4 and treated the cells with CHX (50  $\mu$ g/mL) and CPT (0.5  $\mu$ M). Cells were harvested at the indicated time points for WB.

(N) Western blots in (K)–(M) were quantified and normalized with the value of the 0-h time point and are shown as a line graph.

(O–Q) 22Rv1 cells transfected with HA-ERG-E4 were treated with vehicle (O), CHK1 inhibitor MK1775 (1  $\mu$ M) (P), or WEE1 inhibitor AZD7762 (1.5  $\mu$ M) (Q) for 12 h, followed by treatment with CHX (50  $\mu$ g/mL) and CPT (0.5  $\mu$ M). Cells were harvested for WB at the indicated time points.

(R) Western blots in (O)–(Q) were quantified and normalized with the value of the 0 h time point and are shown as a line graph.



(legend on next page)

## DISCUSSION

Increasing evidence indicates that TMPRSS2-ERG plays a pivotal role in prostate oncogenesis and progression (Brandi et al., 2018; Cai et al., 2009; Carver et al., 2009; Dellioux et al., 2018; King et al., 2009; Klezovitch et al., 2008; Tomlins et al., 2008), stressing that TMPRSS2-ERG could be a viable therapeutic target in PCa. This notion is supported by a recent study showing that TMPRSS2-ERG fusion-positive PCa can be effectively targeted by peptidomimetic inhibitors of TMPRSS2-ERG (Wang et al., 2017). In the present study we reveal that DNA damage-based therapies including IR and CPT induce proteasomal degradation of TMPRSS2-ERG oncoprotein, and such effect is fully dependent on the intact PTEN and GSK3 $\beta$  signaling (Figure S5, left). Thus, our findings suggest that in a cellular context-dependent manner, TMPRSS2-ERG can be targeted by genotoxic therapies such as radiotherapy for effective treatment of fusion-positive PCa.

A previous study performed in two cohorts of PCa patients showed that TMPRSS2-ERG status is not prognostic following radiotherapy (Dal Pra et al., 2013), suggesting that TMPRSS2-ERG fusion-positive PCa is not clinically more sensitive to radiotherapy. In the present study, we provide evidence that although genotoxic therapies induce proteasomal degradation of TMPRSS2-ERG protein, such effect is abolished in PCa cells with PTEN mutation or deletion, phosphorylated or inactivated GSK3 $\beta$ , or FBW7 depletion. These findings are highly relevant because the *PTEN* gene is frequently mutated and/or deletion in PCa, especially at the advanced stage. GSK3 $\beta$  is also often inactivated because of S9 phosphorylation mediated by activated AKT in PTEN-null PCa cells. FBW7 is a known tumor suppressor that is frequently mutated or downregulated in many types of human cancers (Akhoondi et al., 2007). Thus, our findings support the notion that it may be worthwhile to revisit the prognostic value of TMPRSS2-ERG in clinical settings by re-assessing how PCa patients respond differently to radiotherapy according to the status of *PTEN* gene mutation or deletion, GSK3 $\beta$  phosphorylation, and/or FBW7 mutation or downregulation (Figure S5, right).

Increasing evidence indicates that protein stability is critical for the oncogenic activity of ERG, and targeting ERG protein degra-

ation appears to be a promising strategy for PCa therapy (An et al., 2015; Duan and Pagano, 2015; Gan et al., 2015; Wang et al., 2014, 2017). The CULLIN3-based E3 ubiquitin ligase adaptor protein SPOP binds to and promotes proteasomal degradation of WT ERG, but not the truncated oncogenic TMPRSS2-ERG in cells without DNA damage (An et al., 2015; Gan et al., 2015). Through unbiased phage library screen, a few ERG-inhibitory peptides (EIPs) have been identified (Wang et al., 2017). Notably, EIPs preferentially bind to the truncated TMPRSS2-ERG and achieve therapeutic effect in PCa cells by inducing proteasomal degradation of TMPRSS2-ERG proteins (Wang et al., 2017). Thus, EIP-induced TMPRSS2-ERG degradation unlikely mediated by SPOP, but it remains to be determined which E3 ubiquitin ligase(s) are responsible for this process. Additionally, it has been shown that the deubiquitinase enzyme USP9X can stabilize both WT and oncogenic ERG, and the USP9X inhibitor inhibits TMPRSS2-ERG-positive PCa cell growth *in vitro* and *in vivo* by inducing ERG protein degradation (Wang et al., 2014), highlighting that targeting ERG degradation via inhibition of deubiquitinases represents another viable option for treatment of ERG fusion-positive PCa. Further studies have shown that the E3 ubiquitin ligase TRIM25 constitutively binds to and induces proteasomal degradation of both WT and oncogenic ERG in PCa cells (Wang et al., 2016). Intriguingly, increased expression of ERG causes elevation in TRIM25 expression and activity, which is mitigated by USP9X (Wang et al., 2016). Different from SPOP and TRIM25, FBW7 is a signaling-dependent E3 ligase (Welcker and Clurman, 2008). We provide evidence that FBW7-mediated degradation of ERG (both WT and TMPRSS2-ERG) must be primed by ERG protein phosphorylation triggered by DNA damage signaling. Thus, in addition to DNA damage, FBW7 may also play an important role in destruction of oncogenic ERG proteins induced by other signaling pathways, such as those triggered by EIP treatment.

To date, several oncoproteins have been identified as degradation substrates of FBW7, including MYC, c-JUN, CYCLIN E, and NOTCH1. Notably, these proteins invariably contain a consensus FBW7-binding degron (or CPD) I/P/L-pT-P-X-X-pS/E (Aifantis et al., 2008; Welcker and Clurman, 2008)

## Figure 5. FBW7 Mediates ERG Degradation in Response to DNA Damage

- (A) Protein sequence alignment of the region (amino acids 185–193) in ERG with the FBW7-binding motif (degron) identified in the known substrates of FBW7. The lowercase p with a circle refers to the phosphorylation site.
- (B) Protein sequence comparison of the CPD-like motif (red) in ERG protein from different species.
- (C) VCaP cells were treated with CPT (0.5  $\mu$ M) and MG132 (20  $\mu$ M) for 8 h followed by reciprocal colP and WB.
- (D) Control or FBW7-specific knockdown 22Rv1 cells were transfected with HA-ERG-E4 and treated with CPT (0.5  $\mu$ M) and MG132 (20  $\mu$ M) for 8 h followed by colP and WB. ERK2 serves as a loading control.
- (E) 22Rv1 cells were transfected with the indicated plasmids and treated with CPT (0.5  $\mu$ M) for 8 h followed by WB.
- (F) VCaP cells were transfected with FLAG-FBW7 and treated with or without CPT (0.5  $\mu$ M) for 8 h followed by WB.
- (G) Control or FBW7-specific knockdown VCaP cells were treated with CPT (0.5  $\mu$ M) and MG132 (20  $\mu$ M) for 8 h followed by colP and WB. ERK2 serves as a loading control.
- (H) Control or FBW7-specific knockdown 22Rv1 cells were transfected with HA-ERG-E4 and with or without Myc-FBW7. Cells were treated with CPT (0.5  $\mu$ M) and MG132 (20  $\mu$ M) for 8 h followed by colP and WB.
- (I) Control or FBW7 knockdown 22Rv1 cells were transfected with HA-ERG-E4 and treated with CHX (50  $\mu$ g/mL) and CPT (0.5  $\mu$ M). Cells were harvested at the indicated time points for WB.
- (J) Western blots in (I) were quantified and normalized with the value of the 0 h time point and are shown as a line graph.
- (K) 22Rv1 cells were transfected with HA-ERG-E4 in combination with or without FLAG-FBW7. Cells were treated the cells with CHX (50  $\mu$ g/mL) and CPT (0.5  $\mu$ M) followed by WB.
- (L) Western blots in (K) were quantified and normalized with the value of the 0 h time point and are shown as a line graph.



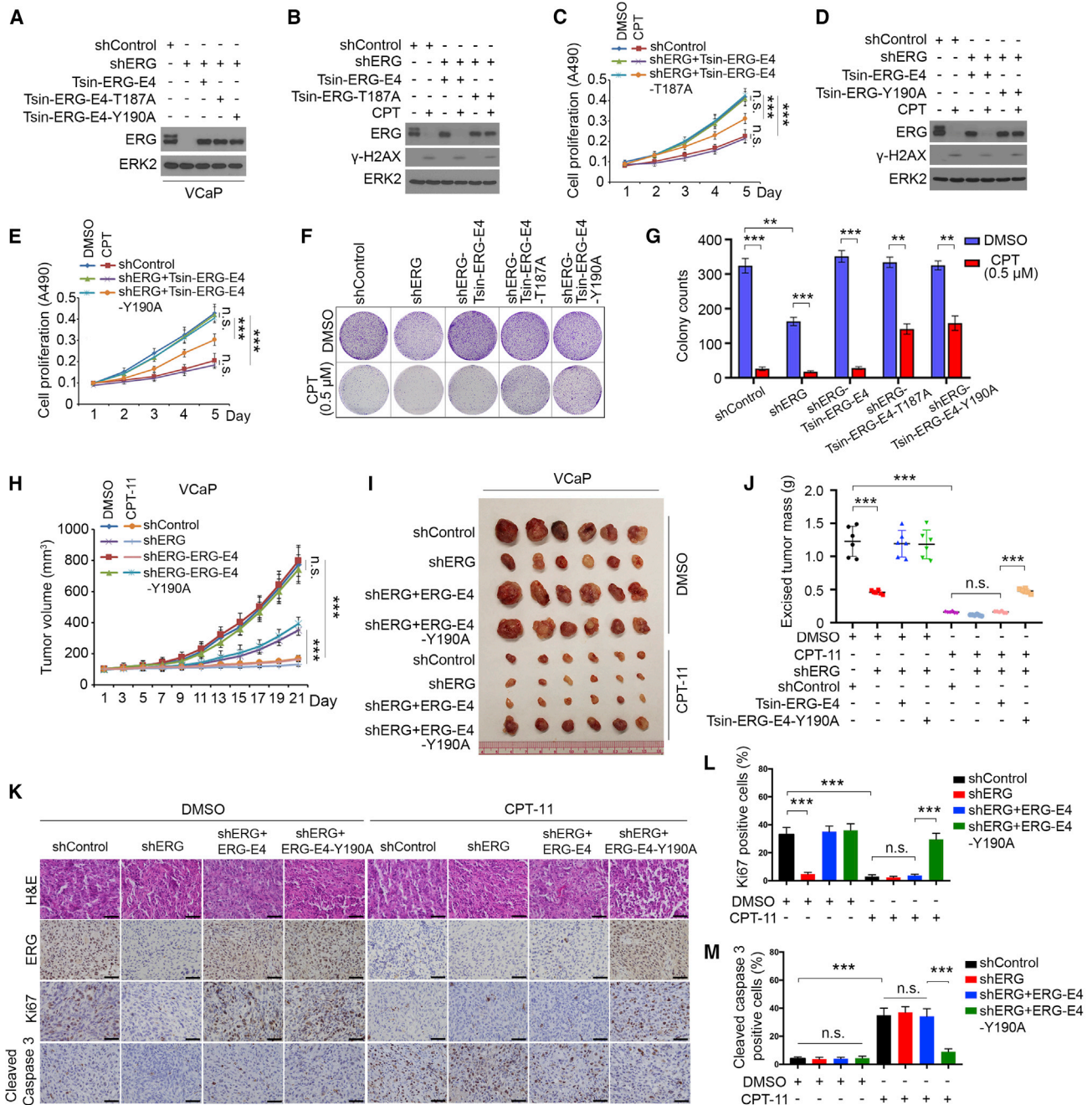


**Figure 7. Degradation-Resistant ERG Confers Resistance to Genotoxic Treatment of PCa Cells in Culture and in Mice**

(A–E) VCaP cells were infected lentivirus expressing the indicated plasmids and treated with or without CPT (0.5 μM) and were harvested for either WB at 8 h post-CPT treatment (A, B, and D) or MTS assay (C and E). Data are shown as mean value ± SD. \*\*\*p < 0.001 and n.s., not significant (unpaired two-tailed Student’s t test).

(F and G) Cells as generated in (A) were treated with or without CPT (0.5 μM) for colony formation assay for 2 weeks (F), and colony numbers were quantified (G). Three independent experiments were conducted. Data are shown as mean value ± SD. \*\*p < 0.01 and \*\*\*p < 0.001 (unpaired two-tailed Student’s t test).

(H–J) Stable cell lines as generated in (A) were mixed with Matrigel and injected subcutaneously into the left and right dorsal flanks of NOD-SCID mice. When the average size of tumors reached 100 mm<sup>3</sup>, mice were treated intraperitoneally (i.p.) with CPT-11 (10 mg/kg) every 2 days, and tumor growth was measured (H). Tumors were harvested at day 21 and photographed (I), and tumor weight (J) was measured. Data are shown as mean value ± SD. \*\*\*p < 0.001 and n.s., not significant (unpaired two-tailed Student’s t test).

(K) H&E staining and IHC staining for ERG, Ki67, and cleaved caspase-3 were performed. Representative images were taken from each group (n = 6). Scale bars are indicated in the images. Scale bar: 50 μm.

(L and M) Ki67 (L) and cleaved caspase-3 (M) positive cells in tissues obtained from (K) were quantified. The number of positive cells from at least five fields was counted and analyzed. Data are shown as mean value ± SD. \*\*\*p < 0.001 and n.s., no significant (unpaired two-tailed Student’s t test).

a phosphorylatable tyrosine (Y) (Figure 5A). Most important, we provide evidence that conversion of T187 and Y190 to non-phosphorylatable alanine abolishes ERG recognition by FBW7 and DNA damage-induced ERG degradation. These findings suggest that similar to the proteins containing the consensus CPD motif I/P/L-pT-P-X-X-pS/E, those possessing the CPD-like variant pT-P-X-pY could also be a prey of FBW7. Therefore, the pT-P-X-pY motif identified in ERG may represent a new class of degron present in FBW7 degradation substrates that have yet been fully unfolded.

In summary, we demonstrate that genotoxic therapies such as radiotherapy induce degradation of oncogenic TMPRSS2-ERG protein in a manner dependent on SCF<sup>FBW7</sup>. Although there is no consensus FBW7-binding/CPD motif I/P/L-pT-P-X-X-pS/E in ERG, we identify a CPD-like variant <sup>187</sup>T-P-X-Y<sup>190</sup>, in which phosphorylation of both T187 and Y190 is important for FBW7-mediated degradation of ERG in response to DNA damage. These data suggest that FBW7 may use the CPD variant as a new means to target proteins for destruction. Our findings also suggest that anti-cancer therapeutics such as radiotherapy can be used to target TMPRSS2-ERG oncoprotein for the treatment of fusion-positive PCa. Given that DNA damage-induced ERG degradation is abolished in cells with PTEN defects, GSK3 $\beta$  phosphorylation or inactivation, or decreased expression of FBW7, it is likely that the prognostic value of TMPRSS2-ERG oncoprotein for DNA damage-based therapies such as radiotherapy of PCa is context dependent, and therefore the significance of our findings warrants further investigation in the clinic setting.

## STAR★METHODS

Detailed methods are provided in the online version of this paper and include the following:

- **KEY RESOURCE TABLE**
- **RESOURCE AVAILABILITY**
  - Lead Contact
  - Materials Availability
  - Data and Code Availability
- **EXPERIMENTAL MODEL AND SUBJECT DETAILS**
  - Cell lines and cell culture
  - Stable cell line generation
- **METHOD DETAILS**
  - Co-immunoprecipitation (coIP) and western blot (WB)
  - Quantitative real-time polymerase chain reaction (qRT-PCR)
  - Chromatin immunoprecipitation and quantitative PCR (ChIP-qPCR)
  - MTS cell proliferation assay
  - Glutathione S-transferase (GST) pull-down assay
  - *In vitro* kinase assay
  - Mouse xenograft and tumor analysis
  - Hematoxylin and eosin (H&E) staining and immunohistochemistry (IHC)
  - Colony formation assay
- **QUANTIFICATION AND STATISTICAL ANALYSIS**
  - Protein quantification
  - Statistical analysis

## SUPPLEMENTAL INFORMATION

Supplemental Information can be found online at <https://doi.org/10.1016/j.molcel.2020.07.028>.

## ACKNOWLEDGMENTS

This work was supported by the Mayo Clinic Foundation, USA (to H.H.).

## AUTHOR CONTRIBUTIONS

H.H. conceived the study. Z Hong, W.Z., D.D., Z. Huang, Y.Y., W.C., Y.P., X.H., S.J.W., R.J.K., D.Wang, and Q.W. generated reagents and conducted experiment design and execution, data collection, and analysis. H.H., Z. Hong, D. Wu, and Q.W. wrote the manuscript.

## DECLARATION OF INTERESTS

The authors declare no competing interests.

Received: May 18, 2020

Revised: July 2, 2020

Accepted: July 29, 2020

Published: August 31, 2020

## REFERENCES

- Adamo, P., and Ladomery, M.R. (2016). The oncogene ERG: a key factor in prostate cancer. *Oncogene* 35, 403–414.
- Aifantis, I., Raetz, E., and Buonamici, S. (2008). Molecular pathogenesis of T-cell leukaemia and lymphoma. *Nat. Rev. Immunol.* 8, 380–390.
- Akhoondi, S., Sun, D., von der Lehr, N., Apostolidou, S., Klotz, K., Maljukova, A., Cepeda, D., Fiegl, H., Dafou, D., Marth, C., et al. (2007). FBXW7/hCDC4 is a general tumor suppressor in human cancer. *Cancer Res.* 67, 9006–9012.
- An, J., Ren, S., Murphy, S.J., Dalangood, S., Chang, C., Pang, X., Cui, Y., Wang, L., Pan, Y., Zhang, X., et al. (2015). Truncated ERG oncoproteins from TMPRSS2-ERG fusions are resistant to SPOP-mediated proteasome degradation. *Mol. Cell* 59, 904–916.
- Attard, G., Cooper, C.S., and de Bono, J.S. (2009). Steroid hormone receptors in prostate cancer: a hard habit to break? *Cancer Cell* 16, 458–462.
- Blee, A.M., He, Y., Yang, Y., Ye, Z., Yan, Y., Pan, Y., Ma, T., Dugdale, J., Kuehn, E., Kohli, M., et al. (2018). Controls luminal epithelial lineage and anti-androgen sensitivity in PTEN and TP53-mutated prostate cancer. *Clin. Cancer Res.* 24, 4551–4565.
- Brandi, F., Grupp, K., Hube-Magg, C., Kluth, M., Lang, D., Minner, S., Möller-Koop, C., Graefen, M., Heinzer, H., Tsourlakis, M.C., et al. (2018). High concordance of TMPRSS-ERG fusion between primary prostate cancer and its lymph node metastases. *Oncol. Lett.* 16, 6238–6244.
- Brenner, J.C., Ateeq, B., Li, Y., Yocum, A.K., Cao, Q., Asangani, I.A., Patel, S., Wang, X., Liang, H., Yu, J., et al. (2011). Mechanistic rationale for inhibition of poly(ADP-ribose) polymerase in ETS gene fusion-positive prostate cancer. *Cancer Cell* 19, 664–678.
- Cai, C., Wang, H., Xu, Y., Chen, S., and Balk, S.P. (2009). Reactivation of androgen receptor-regulated TMPRSS2:ERG gene expression in castration-resistant prostate cancer. *Cancer Res.* 69, 6027–6032.
- Cancer Genome Atlas Research Network (2015). The molecular taxonomy of primary prostate cancer. *Cell* 163, 1011–1025.
- Carrassa, L., and Damia, G. (2017). DNA damage response inhibitors: mechanisms and potential applications in cancer therapy. *Cancer Treat. Rev.* 60, 139–151.
- Carver, B.S., Tran, J., Gopalan, A., Chen, Z., Shaikh, S., Carracedo, A., Alimonti, A., Nardella, C., Varmeh, S., Scardino, P.T., et al. (2009). Aberrant ERG expression cooperates with loss of PTEN to promote cancer progression in the prostate. *Nat. Genet.* 41, 619–624.

- Clark, J., Merson, S., Jhavar, S., Flohr, P., Edwards, S., Foster, C.S., Eeles, R., Martin, F.L., Phillips, D.H., Crundwell, M., et al. (2007). Diversity of TMPRSS2-ERG fusion transcripts in the human prostate. *Oncogene* **26**, 2667–2673.
- Dal Pra, A., Lalonde, E., Sykes, J., Warde, F., Ishkanian, A., Meng, A., Maloff, C., Srigley, J., Joshua, A.M., Petrovics, G., et al. (2013). TMPRSS2-ERG status is not prognostic following prostate cancer radiotherapy: implications for fusion status and DSB repair. *Clin. Cancer Res.* **19**, 5202–5209.
- Delliaux, C., Tian, T.V., Buchet, M., Fradet, A., Vanpouille, N., Flourens, A., Deplus, R., Villers, A., Leroy, X., Clézardin, P., et al. (2018). TMPRSS2:ERG gene fusion expression regulates bone markers and enhances the osteoblastic phenotype of prostate cancer bone metastases. *Cancer Lett.* **438**, 32–43.
- Duan, S., and Pagano, M. (2015). SPOP mutations or ERG rearrangements result in enhanced levels of ERG to promote cell invasion in prostate cancer. *Mol. Cell* **59**, 883–884.
- Fuchs, S.Y., Spiegelman, V.S., and Kumar, K.G. (2004). The many faces of beta-TrCP E3 ubiquitin ligases: reflections in the magic mirror of cancer. *Oncogene* **23**, 2028–2036.
- Gan, W., Dai, X., Lunardi, A., Li, Z., Inuzuka, H., Liu, P., Varmeh, S., Zhang, J., Cheng, L., Sun, Y., et al. (2015). SPOP promotes ubiquitination and degradation of the ERG oncoprotein to suppress prostate cancer progression. *Mol. Cell* **59**, 917–930.
- Giráldez, S., Herrero-Ruiz, J., Mora-Santos, M., Japón, M.A., Tortolero, M., and Romero, F. (2014). SCF(FBXW7 $\alpha$ ) modulates the intra-S-phase DNA-damage checkpoint by regulating Polo like kinase-1 stability. *Oncotarget* **5**, 4370–4383.
- Grabocka, E., Comisso, C., and Bar-Sagi, D. (2015). Molecular pathways: targeting the dependence of mutant RAS cancers on the DNA damage response. *Clin. Cancer Res.* **21**, 1243–1247.
- Gupta-Rossi, N., Le Bail, O., Gonen, H., Brou, C., Logeat, F., Six, E., Ciechanover, A., and Israël, A. (2001). Functional interaction between SEL-10, an F-box protein, and the nuclear form of activated Notch1 receptor. *J. Biol. Chem.* **276**, 34371–34378.
- Hermida, M.A., Dinesh Kumar, J., and Leslie, N.R. (2017). GSK3 and its interactions with the PI3K/AKT/mTOR signalling network. *Adv. Biol. Regul.* **65**, 5–15.
- Hong, X., Liu, W., Song, R., Shah, J.J., Feng, X., Tsang, C.K., Morgan, K.M., Bunting, S.F., Inuzuka, H., Zheng, X.F., et al. (2016). SOX9 is targeted for proteasomal degradation by the E3 ligase FBW7 in response to DNA damage. *Nucleic Acids Res.* **44**, 8855–8869.
- King, J.C., Xu, J., Wongvipat, J., Hieronymus, H., Carver, B.S., Leung, D.H., Taylor, B.S., Sander, C., Cardiff, R.D., Couto, S.S., et al. (2009). Cooperativity of TMPRSS2-ERG with PI3-kinase pathway activation in prostate oncogenesis. *Nat. Genet.* **41**, 524–526.
- Klezovitch, O., Risk, M., Coleman, I., Lucas, J.M., Null, M., True, L.D., Nelson, P.S., and Vasioukhin, V. (2008). A causal role for ERG in neoplastic transformation of prostate epithelium. *Proc. Natl. Acad. Sci. U S A* **105**, 2105–2110.
- Kumar-Sinha, C., Tomlins, S.A., and Chinnaiyan, A.M. (2008). Recurrent gene fusions in prostate cancer. *Nat. Rev. Cancer* **8**, 497–511.
- Lee, J., Kumagai, A., and Dunphy, W.G. (2001). Positive regulation of Wee1 by Chk1 and 14-3-3 proteins. *Mol. Biol. Cell* **12**, 551–563.
- Lin, A.B., McNeely, S.C., and Beckmann, R.P. (2017). Achieving precision death with cell-cycle inhibitors that target DNA replication and repair. *Clin. Cancer Res.* **23**, 3232–3240.
- Lu, K.P., Liou, Y.-C., and Zhou, X.Z. (2002). Pinning down proline-directed phosphorylation signaling. *Trends Cell Biol.* **12**, 164–172.
- Maréchal, A., and Zou, L. (2013). DNA damage sensing by the ATM and ATR kinases. *Cold Spring Harb. Perspect. Biol.* **5**, a012716.
- Minella, A.C., and Clurman, B.E. (2005). Mechanisms of tumor suppression by the SCF(Fbw7). *Cell Cycle* **4**, 1356–1359.
- Nateri, A.S., Riera-Sans, L., Da Costa, C., and Behrens, A. (2004). The ubiquitin ligase SCFFbw7 antagonizes apoptotic JNK signaling. *Science* **303**, 1374–1378.
- Parker, L.L., and Piwnica-Worms, H. (1992). Inactivation of the p34cdc2-cyclin B complex by the human WEE1 tyrosine kinase. *Science* **257**, 1955–1957.
- Robertson, H., Hayes, J.D., and Sutherland, C. (2018). A partnership with the proteasome; the destructive nature of GSK3. *Biochem. Pharmacol.* **147**, 77–92.
- Saura, C., Roda, D., Roselló, S., Oliveira, M., Macarulla, T., Pérez-Fidalgo, J.A., Morales-Barrera, R., Sanchis-García, J.M., Musib, L., Budha, N., et al. (2017). A first-in-human phase I study of the ATP-competitive AKT inhibitor ipatasertib demonstrates robust and safe targeting of AKT in patients with solid tumors. *Cancer Discov.* **7**, 102–113.
- Shimizu, K., Nihira, N.T., Inuzuka, H., and Wei, W. (2018). Physiological functions of FBW7 in cancer and metabolism. *Cell. Signal.* **46**, 15–22.
- Siegel, R.L., Miller, K.D., and Jemal, A. (2016). Cancer statistics, 2016. *CA Cancer J. Clin.* **66**, 7–30.
- Smith, J., Tho, L.M., Xu, N., and Gillespie, D.A. (2010). The ATM-Chk2 and ATR-Chk1 pathways in DNA damage signaling and cancer. *Adv. Cancer Res.* **108**, 73–112.
- Tian, T.V., Tomavo, N., Huot, L., Flourens, A., Bonnelye, E., Flajollet, S., Hot, D., Leroy, X., de Launoit, Y., and Duterque-Coquillaud, M. (2014). Identification of novel TMPRSS2:ERG mechanisms in prostate cancer metastasis: involvement of MMP9 and PLXNA2. *Oncogene* **33**, 2204–2214.
- Tomlins, S.A., Rhodes, D.R., Perner, S., Dhanasekaran, S.M., Mehra, R., Sun, X.W., Varambally, S., Cao, X., Tchinda, J., Kuefer, R., et al. (2005). Recurrent fusion of TMPRSS2 and ETS transcription factor genes in prostate cancer. *Science* **310**, 644–648.
- Tomlins, S.A., Laxman, B., Varambally, S., Cao, X., Yu, J., Helgeson, B.E., Cao, Q., Prensner, J.R., Rubin, M.A., Shah, R.B., et al. (2008). Role of the TMPRSS2-ERG gene fusion in prostate cancer. *Neoplasia* **10**, 177–188.
- van Weeren, P.C., de Bruyn, K.M., de Vries-Smits, A.M., van Lint, J., and Burgering, B.M. (1998). Essential role for protein kinase B (PKB) in insulin-induced glycogen synthase kinase 3 inactivation. Characterization of dominant-negative mutant of PKB. *J. Biol. Chem.* **273**, 13150–13156.
- Wang, J., Cai, Y., Yu, W., Ren, C., Spencer, D.M., and Iltmann, M. (2008). Pleiotropic biological activities of alternatively spliced TMPRSS2/ERG fusion gene transcripts. *Cancer Res.* **68**, 8516–8524.
- Wang, S., Kollipara, R.K., Srivastava, N., Li, R., Ravindranathan, P., Hernandez, E., Freeman, E., Humphries, C.G., Kapur, P., Lotan, Y., et al. (2014). Ablation of the oncogenic transcription factor ERG by deubiquitinase inhibition in prostate cancer. *Proc. Natl. Acad. Sci. U S A* **111**, 4251–4256.
- Wang, S., Kollipara, R.K., Humphries, C.G., Ma, S.-H., Hutchinson, R., Li, R., Siddiqui, J., Tomlins, S.A., Raj, G.V., and Kittler, R. (2016). The ubiquitin ligase TRIM25 targets ERG for degradation in prostate cancer. *Oncotarget* **7**, 64921–64931.
- Wang, X., Qiao, Y., Asangani, I.A., Ateeq, B., Poliakov, A., Cieslik, M., Pitschiya, S., Chakravarthi, B., Cao, X., Jing, X., et al. (2017). Development of peptidomimetic inhibitors of the ERG gene fusion product in prostate cancer. *Cancer Cell* **31**, 532–548.e7.
- Welcker, M., and Clurman, B.E. (2008). FBW7 ubiquitin ligase: a tumour suppressor at the crossroads of cell division, growth and differentiation. *Nat. Rev. Cancer* **8**, 83–93.
- Welcker, M., Orian, A., Ji, J., Grim, J.A., Harper, J.W., Eisenman, R.N., and Clurman, B.E. (2005). The Fbw7 tumor suppressor regulates glycogen synthase kinase 3 phosphorylation-dependent c-Myc protein degradation. *Proc. Natl. Acad. Sci. U S A* **103**, 504–504.
- Yada, M., Hatakeyama, S., Kamura, T., Nishiyama, M., Tsunematsu, R., Imaki, H., Ishida, N., Okumura, F., Nakayama, K., and Nakayama, K.I. (2004). Phosphorylation-dependent degradation of c-Myc is mediated by the F-box protein Fbw7. *EMBO J.* **23**, 2116–2125.
- Yang, Y., Blee, A.M., Wang, D., An, J., Pan, Y., Yan, Y., Ma, T., He, Y., Dugdale, J., Hou, X., et al. (2017). Loss of FOXO1 cooperates with TMPRSS2-ERG overexpression to promote prostate tumorigenesis and cell invasion. *Cancer Res.* **77**, 6524–6537.

Ye, X., Nalepa, G., Welcker, M., Kessler, B.M., Spooner, E., Qin, J., Elledge, S.J., Clurman, B.E., and Harper, J.W. (2004). Recognition of phosphodegron motifs in human cyclin E by the SCF(Fbw7) ubiquitin ligase. *J. Biol. Chem.* 279, 50110–50119.

Zhang, H., Pan, Y., Zheng, L., Choe, C., Lindgren, B., Jensen, E.D., Westendorf, J.J., Cheng, L., and Huang, H. (2011). FOXO1 inhibits Runx2 transcriptional activity and prostate cancer cell migration and invasion. *Cancer Res.* 71, 3257–3267.

STAR★METHODS

KEY RESOURCE TABLE

REAGENT or RESOURCE	SOURCE	IDENTIFIER
<b>Antibodies</b>		
Rabbit monoclonal anti-ERG	Abcam	Cat# ab92513; RRID: AB_2630401
Mouse monoclonal anti-ERG	Biocare Medical	Cat# CM421C; RRID: AB_10804797
Rabbit polyclonal anti-FBXW7	Abcam	Cat# ab109617; RRID: AB_2687519
Rabbit monoclonal anti-AKT	Cell Signaling Technology	Cat# 9272S; RRID:AB_329827
Rabbit monoclonal anti-Phospho-AKT (Ser473)	Cell Signaling Technology	Cat# 9271S; RRID:AB_329825
Rabbit monoclonal anti-GSK-3 $\beta$	Cell Signaling Technology	Cat# 9315; RRID:AB_490890
Rabbit monoclonal anti-Phospho-GSK-3 $\beta$ (Ser9)	Cell Signaling Technology	Cat# 9322; RRID:AB_2115196
Rabbit polyclonal anti-ATM	Santa-Cruz	Cat# sc-7230; RRID: AB_634181
Rabbit monoclonal anti-ATR	Cell Signaling Technology	Cat# 13934S; RRID: AB_2798347
Rabbit polyclonal anti-CHK1	Santa-Cruz	Cat# sc-7898; RRID: AB_2229488
Rabbit polyclonal anti-Phospho-CHK1 (Ser345)	Cell Signaling Technology	Cat# 2348S; RRID: AB_331212
Rabbit monoclonal anti-CHK2	Cell Signaling Technology	Cat# 6334S; RRID: AB_11178526
Rabbit monoclonal anti-Phospho-CHK2 (Thr68)	Cell Signaling Technology	Cat# 2661S; RRID: AB_331479
Rabbit monoclonal anti-WEE1	Cell Signaling Technology	Cat# 13084S; RRID: AB_2713924
Rabbit monoclonal anti-Phospho-Histone H2A.X (Ser139)	Cell Signaling Technology	Cat# 9718S; RRID: AB_2118009
Rabbit monoclonal anti-PTEN	Cell Signaling Technology	Cat# 9559; RRID: AB_390810
Rabbit polyclonal anti-SPOP	Proteintech	Cat# 16750-1-AP; RRID: AB_2756394
Mouse monoclonal anti-TRIM25	Santa-Cruz	Cat# sc-166926; RRID: AB_10608081
Mouse monoclonal anti-AR	Santa-Cruz	Cat# sc-7305; RRID: AB_626671
Mouse monoclonal anti-ERK2	Santa-Cruz	Cat# sc-135900; RRID: AB_2141283
Mouse monoclonal anti-HA.11	Covance	Cat# MMS-101R; RRID: AB_291262
Mouse monoclonal anti-c-Myc	Santa-Cruz	Cat# sc-40; RRID: AB_627268
Mouse monoclonal anti-FLAG M2	Sigma-Aldrich	Cat# F-3165; RRID: AB_259529
<b>Bacterial and Virus Strains</b>		
<i>E.coli</i> DH5 $\alpha$	Thermo Fisher	Cat#18258012
<i>E.coli</i> BL21	Thermo Fisher	Cat#C600003
Lentivirus-expressing GSK3 $\beta$ -shRNAs	Sigma-Aldrich	SHCLNG-NM_002093
Lentivirus-expressing ATM-shRNAs	Sigma-Aldrich	SHCLNG-NM_000051
Lentivirus-expressing ATR-shRNAs	Sigma-Aldrich	SHCLNG-NM_001184
Lentivirus-expressing CHK1-shRNAs	Sigma-Aldrich	SHCLNG-NM_001274
Lentivirus-expressing CHK2-shRNAs	Sigma-Aldrich	SHCLNG-NM_007194
Lentivirus-expressing WEE1-shRNAs	Sigma-Aldrich	SHCLNG-NM_003390
Lentivirus-expressing FBW7-shRNAs	Sigma-Aldrich	SHCLNG-NM_018315
Lentivirus-expressing ERG-shRNAs	Sigma-Aldrich	SHCLNG-NM_004449
Lentivirus-expressing SPOP-shRNAs	Sigma-Aldrich	SHCLNG-NM_025287
Lentivirus-expressing TRIM25-shRNAs	Sigma-Aldrich	SHCLNG-NM_005082

(Continued on next page)

REAGENT or RESOURCE	SOURCE	IDENTIFIER
<b>Continued</b>		
Chemicals, Peptides, and Recombinant Proteins		
MG132	Sigma-Aldrich	Cat#M8699
Cycloheximide	Sigma-Aldrich	Cat#01810
Lipofectamine 2000 reagent	Thermo Fisher	Cat#11668500
<i>Polyethylenimine</i>	Sigma-Aldrich	Cat#408727
Polybrene	Sigma-Aldrich	Cat#TR-1003-G
Lithium Chloride (LiCl)	Sigma-Aldrich	Cat#L4408
Camptothecin (CPT)	Selleckchem	Cat#S1288
KU-55933	Selleckchem	Cat#S1092
VE-822	Selleckchem	Cat#S7102
CPT-11	Sigma-Aldrich	Cat#I1406
AZD7762	Selleckchem	Cat#S1532
MK-1775	Selleckchem	Cat#S1525
GDC-0068	MedChem Express	Cat# HY-15186A
MK-2206	Selleckchem	Cat#S1078
Critical Commercial Assays		
KOD Plus Mutagenesis Kit	Toyobo	Cat#F0936K
Lambda Protein Phosphatase	NEB	Cat#P0753S
<i>In vitro</i> transcription/translation System	Promega	Cat#L1170
Deposited Data		
Raw data and images	This paper and Mendeley Data	<a href="http://dx.doi.org/10.17632/ph2xvpxs2y.2">http://dx.doi.org/10.17632/ph2xvpxs2y.2</a>
Experimental Models: Cell Lines		
Human: VCaP	ATCC	CRL-2876
Human: 22Rv1	ATCC	CRL-2505
Human: LNCaP	ATCC	CRL-1740
Human: C4-2	Uro Corporation	N/A
Human: DU145	ATCC	HTB-81
Human: PC-3	ATCC	CRL-1435
Human: HEK293T	ATCC	CRL-11268
Oligonucleotides		
See <a href="#">Table S1</a> for sh-RNAs sequences; See <a href="#">Tables S2</a> and <a href="#">S3</a> for primer sequences		N/A
Software and Algorithms		
ImageJ	NIH	<a href="https://imagej.nih.gov/ij/index.html">https://imagej.nih.gov/ij/index.html</a>
GraphPad Prism 7.0	Graphpad, Inc	<a href="https://www.graphpad.com">https://www.graphpad.com</a>

## RESOURCE AVAILABILITY

### Lead Contact

Further information and requests for resources and reagents should be directed to and will be fulfilled by the Lead Contact Haojie Huang ([huang.haojie@mayo.edu](mailto:huang.haojie@mayo.edu)).

### Materials Availability

All the reagents and materials generated in this study are available from the Lead Contact without restriction.

### Data and Code Availability

The dataset supporting the current study have been deposited in a public repository (Mendeley Data): <https://doi.org/10.17632/ph2xvpxs2y.1>.

## EXPERIMENTAL MODEL AND SUBJECT DETAILS

### Cell lines and cell culture

LNCaP, 22Rv1, PC-3, DU145, VCaP, HEK293T cell lines were purchased from the American Type Culture Collection (ATCC). C4-2 cell line was purchased from Uro Corporation. LNCaP, C4-2, PC-3, DU145 and 22Rv1 cells were cultured in RPMI-1640 cell culture medium (Corning) containing 10% fetal bovine serum (FBS), together with 100  $\mu\text{g}/\text{ml}$  streptomycin and 100 U/ml penicillin. VCaP cells were cultured in DMEM cell culture medium (Corning) containing 13% FBS, together with 100  $\mu\text{g}/\text{ml}$  streptomycin and 100 U/ml penicillin. HEK293T cells were cultured in DMEM cell culture medium (Corning) containing 10% FBS, together with 100  $\mu\text{g}/\text{ml}$  streptomycin and 100 U/ml penicillin. All cell lines were authenticated by STR profiling and cultured in incubator with 37°C and 5% CO<sub>2</sub>.

### Stable cell line generation

Lentivirus transduction system was utilized to generate stable cell lines with specific gene knockdown or overexpression. PEI was used to transfect shRNA plasmids together with lentivirus package plasmids (PSPAX2 and PMD2.G) into HEK293T cells. 48 h after transfection, supernatant containing viruses was collected, filtered and utilized to infect indicated cells. Polybrene (8  $\mu\text{g}/\text{ml}$ ) was added to the viral supernatant to increase the infection efficiency. 48 h after infection, culture medium was replaced with fresh medium, and puromycin (1.5  $\mu\text{g}/\text{ml}$ ) was administered for cell selection. shRNA sequence information is provided in [Table S1](#).

## METHOD DETAILS

### Co-immunoprecipitation (coIP) and western blot (WB)

For coIP assay, cells were lysed with IP buffer (150 mM NaCl, 50 mM Tris-HCl pH = 7.5, 1% Nonidet P-40, 0.5% sodium deoxycholate and 1% protease inhibitor cocktails) for 30 min, and cell lysate was harvested by centrifuging followed by incubation with indicated antibodies and Protein G Plus/Protein A agarose beads (Sigma-Aldrich, USA) at 4°C overnight. Next day, the beads with target proteins linked on it were washed 6 times with IP buffer. Proteins were denatured for western blot analysis. For WB, target proteins were denatured using sample buffer supplied with 10% DTT (Thermo Fisher Scientific, USA) and boiled at 95°C for 10 min. Samples were subjected to SDS-polyacrylamide gel (Bio-Rad, USA) separation, and the gels were further transferred to nitrocellulose (NC) membranes (Thermo Fisher Scientific, USA). After transferring, the NC membranes were blocked in 5% non-fat milk (Bio-Rad, USA) for 1 h at room temperature and incubated with the indicated primary antibodies at 4°C overnight. Next day, the NC membranes were washed with 1 × TBST for 10 min three times and incubated with matched secondary antibody for 1 h at room temperature. The membranes were washed with 1 × TBST for 10 min for another three times. Lastly, the signals were developed with SuperSignal West Pico Luminal Enhancer Solution (Thermo Fisher Scientific, USA) on autoradiography films (HyBlot CL, USA).

### Quantitative real-time polymerase chain reaction (qRT-PCR)

Total RNA was extracted from the cells by utilizing Trizol reagent (Ambion, USA) and reversely transcribed into cDNA by utilizing the GoScript kit (Promega, USA). The SYBR-green Mix (Bio-Rad, USA) and CFX96 Real-Time System (Bio-Rad, USA) were utilized to conduct the real-time PCR according to manufacturer's instruction. Expression of *GAPDH* gene was used as an inner control. Sequence information for primers used for qRT-PCR is provided in [Table S2](#).

### Chromatin immunoprecipitation and quantitative PCR (ChIP-qPCR)

ChIP-qPCR was performed as previously described ([Yang et al., 2017](#)). Briefly, formaldehyde (11%) solution was utilized to crosslink chromatin in cells for 10 min at room temperature. Crosslinked chromatin was sonicated, and immunoprecipitated with Protein G Plus/Protein A agarose beads (Sigma-Aldrich, USA) together with indicated antibody at 4°C overnight. The Protein-DNA complexes were precipitated and eluted and cross-linking was reversed at 65°C for 16 h. DNA fragments were purified and analyzed by real-time PCR. Sequence information for primers used for ChIP-qPCR is provided in [Table S3](#).

### MTS cell proliferation assay

Cell proliferation was measured utilizing the MTS assay (Promega, USA) according to manufacturer's instruction. Briefly, cells were seeded in a 96-well plate with a density of 1,000 cells per well. At the indicated time points, 20  $\mu\text{l}$  CellTiter 96R Aqueous One Solution reagent (Promega, USA) was added to cells. After incubating at 37°C incubator for 1 h, cell growth was measured in a microplate reader with absorbance at 490 nm. The values of each time points are normalized with the value of 0 h and shown in fold change.

### Glutathione S-transferase (GST) pull-down assay

Cells were lysed with IP buffer (50 mM Tris-HCl, pH 7.4, 1% Triton X-100, 150 mM NaCl, 1% sodium deoxycholate and 1% protease inhibitor cocktails) on ice for 30 min. GST fusion proteins were immobilized on glutathione-Sepharose beads (GE Healthcare Life-sciences). After washing with lysis buffer, the beads were incubated with cell lysates at 4°C overnight. The beads were then washed six times with binding buffer and re-suspended in sample buffer. The bound proteins were subjected to *in vitro* kinase assay.

### **In vitro kinase assay**

Plasmid DNA (T7 promoter-GSK3 $\beta$  or T7 promoter-WEE1) was added to the TNT T7 Quick Master Mix and add 1 mL methionine (1 mM), by following the manufacturer's instruction of TNT Quick Coupled Transcription/Translation Systems (Promega). GST-ERG-E4, GST-ERG-E4-T187A or GST-ERG-E4-Y190A proteins were immobilized on glutathione-Sepharose beads. After washing with PBS, the beads were incubated with *in vitro* transcribed and translated GSK3 $\beta$  or WEE1 kinases, and reaction buffer (25 mM Tris-HCl (pH 7.5), 0.1 mg/ml BSA, 2 mM dithiothreitol (DTT), 0.1 mM Na<sub>3</sub>VO<sub>4</sub>, 5 mM beta-glycerophosphate, 10 mM MgCl<sub>2</sub>, 200  $\mu$ M ATP) at room temperature for 60 min. The beads were then washed six times with PBS and re-suspended in sample buffer. The bound proteins were subjected to western blot analysis.

### **Mouse xenograft and tumor analysis**

NOD-SCID male mice in the age of 6 week old were utilized in this study. All the mice were generated in house and housed in standard condition with a 12-hour light/12-hour dark cycle and access to food and water *ad libitum*. Mice were randomly divided into indicated groups. A total number of  $5 \times 10^6$  22Rv1 cells stably expressing ERG-E4 or mutant were injected subcutaneously into the left and right flanks of mice, together with 50  $\mu$ l Matrigel matrix (BD Bioscience, USA). Growth of xenografts was monitored every two days by calipers externally. Once the tumor size reached 100 mm<sup>3</sup> (approximately 3-5 weeks after injection), CPT-11 (Irinotecan) (10 mg/kg) was injected intraperitoneally into mice every two days, while PBS was injected in the same volume as a control. In due day, mice were sacrificed and tumors were excised for analysis of their sizes and their weights. The protocols for these mice experiments were approved by Mayo Clinic IACUC.

### **Hematoxylin and eosin (H&E) staining and immunohistochemistry (IHC)**

For both H&E staining and IHC staining, xenograft tumor samples were fixed by formalin and embedded into paraffin. Four-micrometer thick sections were cut from the samples and fixed. For H&E staining, xylene was used to deparaffinize the tissues, followed by gradient ethanol washes (100% > 95% > 80% > 70%) to rehydrate them. Tissue samples on slides were stained by hematoxylin, and the slides were washed twice and counterstained with 1% eosin. Stained tissue slides were dehydrated again by gradient ethanol washes and xylene before mounting and sealing with the coverslips. For IHC staining, antigen retrieval and immuno-staining were performed as described previously (Zhang et al., 2011).

### **Colony formation assay**

Cells were re-suspended in culture medium and seeded in 6-well plates with a density of 1,000 cells/well for 22Rv1; 1,500 cells/well for VCaP. Cells were incubated for 2 weeks at 37°C with 5% CO<sub>2</sub>. Culture medium was aspirated and the colonies were washed twice with PBS, and fixed with methanol and acetic acid (1:3) for 2h. The colonies were further stained by 0.5% crystal violet for 4h, and washed with water twice to remove the crystal violet. The number of colonies (the colonies with cell number over 50) in each well was counted.

## **QUANTIFICATION AND STATISTICAL ANALYSIS**

### **Protein quantification**

Protein expression levels were quantified from western blot bands using ImageJ software (software detail refers to the [Key Resources Table](#)). Relative levels for target protein expression were determined by normalizing with the western blot band intensity of control proteins.

### **Statistical analysis**

All data were shown as mean values  $\pm$  SD from three independent experiments. Differences between two groups were analyzed using unpaired Student's t test or ANOVA test. p value < 0.05 was considered statistically significant.